AGU PUBLICATIONS

Global Biogeochemical Cycles

RESEARCH ARTICLE
10.1002/2015GB005355

Key Points:
- Phytoplankton cell size impacts discernable in POC flux data
- Small cells had greater export flux efficiency but lower transfer efficiency
- Large cells were more refractory and sank faster with greater transfer efficiency

Correspondence to:
C. B. Mouw,
cmouw@uri.edu

Citation:
Mouw, C. B., A. Barnett, G. A. McKinley, L. Gloege, and D. Pilcher (2016), Phytoplankton size impact on export flux in the global ocean, *Global Biogeochem. Cycles*, *30*, 1542–1562, doi:10.1002/2015GB005355.

Received 11 DEC 2015
Accepted 12 OCT 2016
Accepted article online 14 OCT 2016
Published online 29 OCT 2016

Phytoplankton size impact on export flux in the global ocean

Colleen B. Mouw[1,2], Audrey Barnett[1,2], Galen A. McKinley[3], Lucas Gloege[3], and Darren Pilcher[4]

[1]Department of Geological and Mining Engineering and Sciences, Michigan Technological University, Houghton, Michigan, USA, [2]Now at Graduate School of Oceanography, University of Rhode Island, Narragansett, Rhode Island, USA, [3]Department of Atmospheric and Oceanic Sciences, University of Wisconsin-Madison, Madison, Wisconsin, USA, [4]NOAA, Pacific Marine Environmental Laboratory, Seattle, Washington, USA

Abstract Efficiency of the biological pump of carbon to the deep ocean depends largely on biologically mediated export of carbon from the surface ocean and its remineralization with depth. Global satellite studies have primarily focused on chlorophyll concentration and net primary production (NPP) to understand the role of phytoplankton in these processes. Recent satellite retrievals of phytoplankton composition now allow for the size of phytoplankton cells to be considered. Here we improve understanding of phytoplankton size structure impacts on particle export, remineralization, and transfer. A global compilation of particulate organic carbon (POC) flux estimated from sediment traps and ^{234}Th are utilized. Annual climatologies of NPP, percent microplankton, and POC flux at four time series locations and within biogeochemical provinces are constructed. Parameters that characterize POC flux versus depth (export flux ratio, labile fraction, and remineralization length scale) are fit for time series locations, biogeochemical provinces, and times of the year dominated by small and large phytoplankton cells where phytoplankton cell size show enough dynamic range over the annual cycle. Considering all data together, our findings support the idea of high export flux but low transfer efficiency in productive regions and vice versa for oligotrophic regions. However, when parsing by dominant size class, we find periods dominated by small cells to have both greater export flux efficiency and lower transfer efficiency than periods when large cells comprise a greater proportion of the phytoplankton community.

1. Introduction

Phytoplankton form the base of the marine food web and play a crucial role in biogeochemical processes, including determining the efficiency of the biological pump that exports carbon to the deep ocean. This latter process is critical for global ocean sequestration of carbon and therefore modulation of atmospheric carbon dioxide. Phytoplankton are extremely diverse in terms of taxonomy, morphology, and size [*Cullen et al*., 2002; *Margalef*, 1978]. They span over 10 orders of magnitude in cell volume, and community size structure is determined by environmental factors such as temperature, nutrient, and light availability. In a sense, community structure can be considered an integrator of environmental factors [*Claustre et al*., 2005]. For example, within the phytoplankton there are strong taxonomic and functional contrasts between blooms of large aggregating and sinking diatoms, and populations of picoplankton tightly coupled with the microbial loop [*Pomeroy*, 1974] where most organic carbon is locally recycled. Small phytoplankton cells dominate in stable oligotrophic environments such as the open ocean, while larger cells can dominate biomass in variable eutrophic environments such as upwelling, high-latitude, and coastal areas [*Chisholm*, 1992; *Malone*, 1980; *Yentsch and Phinney*, 1989]. These contrasts in the function of cell size have been shown to regulate the efficiency of exported organic matter [*Dunne et al*., 2005; *Guidi et al*., 2009].

Particulate organic carbon (POC) flux observations have been made over many decades in the interest of understanding the biological pump of carbon to the deep ocean. The efficiency of this process depends largely on the biologically mediated export of carbon from the surface ocean and its remineralization with depth. While there have been a variety of new techniques to observe POC flux, sediment traps have been the most extensive temporally and geographically. POC flux observations made with sediment traps and optical imaging suggest that ecosystem structure plays an important role in POC flux [*Guidi et al*., 2009; *Buesseler and Boyd*, 2009; *Lam et al*., 2011; *Henson et al*., 2012]. Diatom-dominated phytoplankton communities in productive areas, such as high-latitude environments and upwelling regions, have high export efficiency, but the exported material decays rapidly at depth because it is relatively labile and prone to remineralization in the

upper mesopelagic. This results in a high export efficiency but low transfer efficiency in these regions. Conversely, in lower latitude oligotrophic environments, where diatoms are largely absent, primary production is low and mostly regenerated; consequentially, the small fraction of material that is eventually exported is likely to be refractory and undergo relatively little degradation at depth, resulting in low export efficiency but high transfer efficiency [*Henson et al*., 2012; *Lam et al*., 2011; *Lima et al*., 2014; but see *Marsay et al*., 2015].

Many studies have sought to quantify the impact of phytoplankton community on POC flux observations. These have ranged from investigations that utilize satellite imagery of chlorophyll concentration ([Chl]) and/or net primary production (NPP) to relationships that consider phytoplankton size structure (through high-performance liquid chromatography pigments or particle imaging). The latter suggests that phytoplankton cell size is an important consideration. For example, *Guidi et al*. [2009] suggested that phytoplankton composition explained 68% of the variance in flux at 400 m. *Dunne et al*. [2005] showed biomass controls 59% of the variance in export flux, while size structure is the next most important factor, explaining 28% of the variance. Cell size also has an impact on the remineralization of exported material. *Guidi et al*. [2015] found that exported POC was more refractory and remineralization depths increased as the fraction of microplankton decreased or the fraction of picoplankton increased.

Satellite remote sensing of phytoplankton functional types has recently become an active area of research. Estimates of phytoplankton taxonomic groups, phytoplankton size classes, and particle size distribution can now be made [*IOCCG*, 2014]. *Guidi et al*. [2015] was the first to correlate satellite estimates of phytoplankton size estimated with particle imaging to an empirical coefficient representing remineralization. In the context of these recent advances, we seek to investigate more broadly the connection between phytoplankton size and export flux. We build on *Guidi et al*. [2015] by estimating more parameters through the use of a different fitting model and utilizing a broader POC flux data set. We estimate remineralization along with export efficiency, labile fraction, and absolute exported POC flux dependent on phytoplankton size estimated from satellite imagery. The goal of this study is to improve understanding of how phytoplankton size structure controls particle export and remineralization. *Passow and Carlson* [2012] suggest that the greatest success in understanding export flux processes will be met at the regional scale due to the great diversity in ecosystem-specific food web structure. Thus, we specifically explore the impact of phytoplankton size composition on export flux at key time series sites and within biogeochemical provinces across the global ocean.

2. Methodology

Here we provide a brief outline of data analysis steps with details in the following sections:

1. Field measurements of POC flux from sediment traps and thorium-234 along with paired satellite estimates of primary production and microplankton fraction are collected.
2. Data are grouped into biogeochemical provinces and formed into monthly, depth-binned climatologies for both POC flux and satellite parameters.
3. Climatological years are split into times of large- and small-cell dominance.
4. POC flux climatology versus depth is characterized using the relationship of *Lima et al*. [2014] to retrieve the export flux ratio, remineralization length scale, and refractory fraction.
5. Variability in retrieved parameters is interpreted in relation to ecosystem structure.

2.1. POC Flux Measurements and Satellite Products

We utilize the data set of *Mouw et al*. [2016], a compilation of field estimates of POC flux along with matched satellite data products available on PANGEA (doi.pangaea.de/10.1594/PANGAEA.855600). Briefly described, the data set comprises a total of 15,792 individual POC flux measurements acquired from public repositories and published literature at 673 unique locations with 43% collected after 1997, concurrent with the satellite record. Both sediment trap and ^{234}Th measurements are included to improve the resolution of observations in the upper 500 m of the water column [*Dunne et al*., 2005; *Henson et al*., 2012; *Guidi et al*., 2015], with ^{234}Th representing 4% of the total data set. In the interest of matching the time scale of POC flux to satellite-derived products to the greatest degree possible, we separate a subset from the sediment trap data set where individual trap cup intervals are 30 days or less. The majority of measurements (92%) fall into this category with a median cup interval of 14 days and a standard deviation of 6 days. We utilize all short-deployment POC flux data, regardless of overlap with the satellite record [*Lutz et al*., 2007].

Table 1. Summary of Notation

	Description
$F_{z\text{-}ze}$	POC flux at a depth below the depth of export (mg C m^{-2} d^{-1})
F_{ze}	POC flux at the depth of export (mg C m^{-2} d^{-1})
z_e	Depth of export (m)
p_{ze}	Ratio of POC flux to NPP at the depth of export, also called export flux efficiency (%)
$p_{z\text{-}ze}$	Ratio of POC flux to NPP at a depth below the depth of export (%)
α	Labile fraction of POC (%)
λ	Remineralization length scale (m)
NPP	Vertically integrated net primary production (mg C m^{-2} d^{-1})
S_{fm}	Fraction of microplankton (>20 μm) phytoplankton cells (%)
$TE_{z\text{-}ze}$	Transfer efficiency at a depth below the depth of export (%)

To complement these in situ data, *Mouw et al*. [2016] provide satellite-derived estimates of net primary production (NPP, gC m^{-2} d^{-1}, vertically generalized production model [*Behrenfeld and Falkowski*, 1997]), microplankton fraction (S_{fm}, % [*Mouw and Yoder*, 2010]), and the diffuse attenuation coefficient at 490 nm (K_d(490), m^{-1}). We retrieve the depth of the euphotic zone (z_{eu}, m) from K_d(490) [*O'Reilly et al*., 2000] as 4.6/K_d(490) [*Morel and Berthon*, 1989]. A monthly mixed layer depth (MLD, m) climatology derived from a variable density threshold equivalent to 0.2°C [*de Boyer Montégut et al*., 2004; *de Boyer Montégut et al*., 2007; *Mignot et al*., 2007] is also provided from Ifremer/LOS Mixed Layer Depth Climatology group (www.ifremer.fr/cerweb/deboyer/mld). A summary of notation is found in Table 1.

Deuser et al. [1988] first proposed a "statistical funnel" defining the region of probability at the sea surface likely to contribute to observed particle flux collected by a sediment trap. Subsequent modeling and in situ studies [*Abell et al*., 2013; *Deuser et al*., 1990; *Siegel and Deuser*, 1997] resolve the surface footprint of statistical funnels to be anywhere from 50 km to 500 km in diameter, equivalent to areas ranging between 2000 km^2 and 20,000 km^2. In *Mouw et al*. [2016], satellite data products are retrieved from global 9 km resolution imagery as the median of a 5×5 pixel box centered on each POC flux location [*Bailey and Werdell*, 2006] and are provided as a time series over the complete SeaWiFS mission (Sea-viewing Wide Field-of-view Sensor, September 1997 to December 2010). This is a conservative statistical funnel of 2025 km^2. At the time of writing only 8% of the publically available POC flux observations were measured beyond 2008, when MODIS (Moderate Resolution Imaging Spectroradiometer) replaced the SeaWiFS record; thus, we focus our analysis here solely on SeaWiFS.

2.2. Climatology Construction

While we would prefer to analyze the impact of size on POC flux versus depth at discrete times and locations, the depth resolution of individual POC flux field sites as well as limited temporal overlap with satellite-derived NPP and S_{fm} prevents such an analysis. As previously noted, over half the POC flux data set was collected prior to the satellite record staring in 1997. To improve climatological coverage, we use all short-deployment (<30 days) POC flux observations to construct climatologies, regardless of satellite overlap [*Lutz et al*., 2007].

To characterize average seasonal patterns in regional ecosystems, we construct monthly, depth-binned climatologies for POC flux and satellite data products by pooling data into biogeochemical provinces as defined by *Longhurst* [2006] (provided by *VLIZ* [2009]). *Longhurst* [2006] delineate regions expected to have similar biogeochemical process and ecosystem structure based on the prevailing role of physical forcing as a regulator of phytoplankton distributions. Provinces are defined by considering [Chl], NPP, photic depth, mixed layer depth, and sea surface temperature. Though the physical dynamics governing the boundaries of these provinces vary over time, a static average state is considered here because the sparseness of the POC flux observations does not require dynamic boundaries. Throughout this text, provinces are referred to by their standardized abbreviated short names as found in Figure 1.

With the exception of oceanographic time series locations, the temporal resolution of POC flux measured in the global ocean is limited. Combining data into provincial monthly climatologies better resolves the large-scale average seasonal cycle, but in some cases only a single POC flux measurement may exist across an entire province at a specific depth in a given month. This creates a potential mismatch by pairing episodic events in the POC flux record with well-defined satellite climatology in NPP and S_{fm}. In an effort to mitigate this mismatch, POC flux data are depth binned to combine measurements with similar vertical placement in the water column (e.g., 500 m and 540 m). Depth bins are centered at 20 m, 50 m to 500 m in 50 m increments,

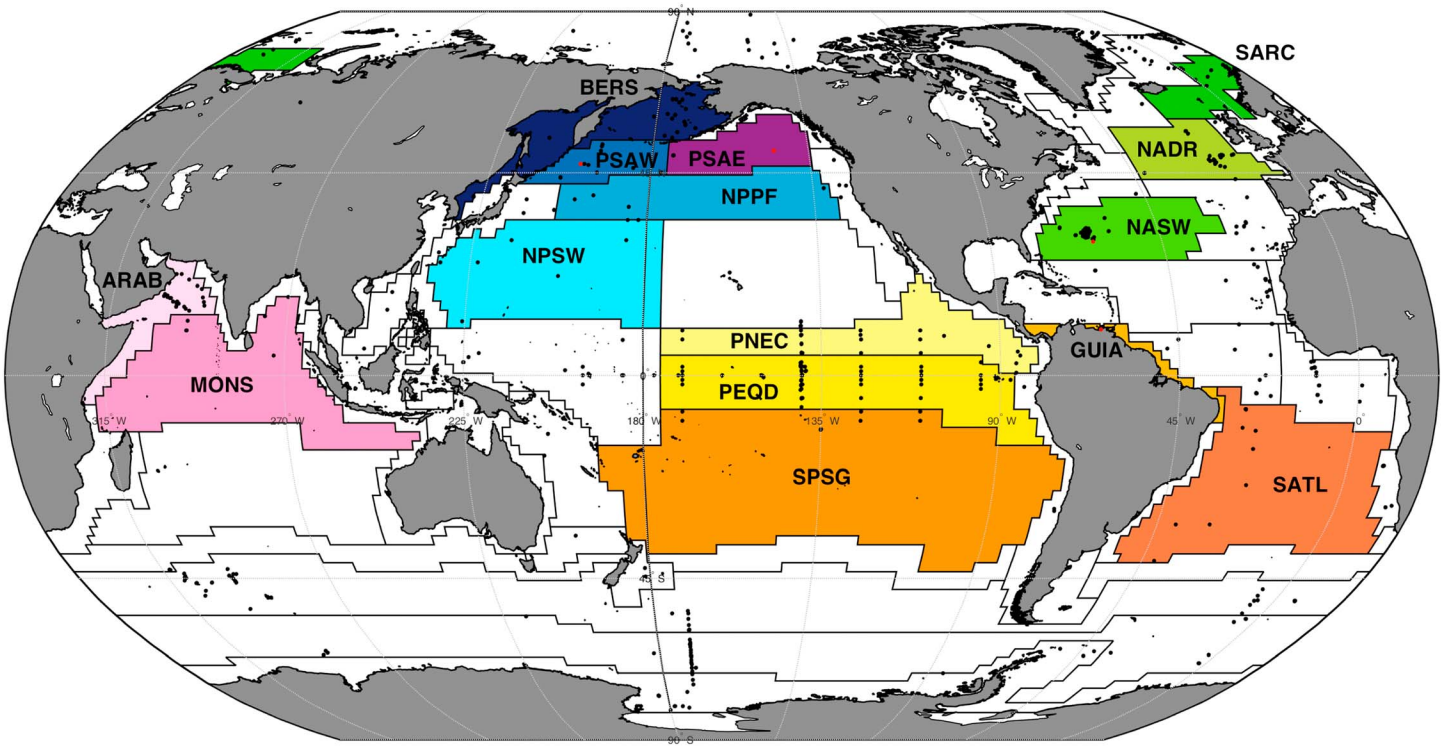

Figure 1. POC flux observation locations (filled circles) overlain with *Longhurst* [2006] provinces. Time series sites are noted with red filled circles. Colored provinces (16 out of 54) indicate where enough POC flux data were present to fit with statistical confidence: the Atlantic Subarctic Province (SARC), North Atlantic Drift Province (NADR), North Atlantic Subtropical Gyre West (NASW), Guianas Coastal Province (GUIA), South Atlantic Gyral Province (SATL), North Pacific Epicontinental Province (BERS), Pacific Subarctic Gyres Province West (PASW), Pacific Subarctic Gyres Province East (PSAE), North Pacific Polar Front Province (NPPF), North Pacific Subtropical Gyre Province West (NPSW), North Pacific Equatorial Countercurrent Province (PNEC), Pacific Equatorial Divergence Province (PEQD), South Pacific Subtropical Gyre Province (SPSG), North West Arabian Upwelling Province (ARAB), and the Indian Monsoon Gyres Province (MONS).

and 500 m to 5000 m in 200 m increments. Spacing is chosen to combine vertically similar measurements to better represent an average climatology while still capturing variability throughout the water column. Across the globe, observed POC flux is much more variable at shallower depths; below 1000 m POC flux is 6 $\pm$ 10 mg C m^{-2} d^{-1} (mean $\pm$ SD) compared with 31 $\pm$ 58 mg C m^{-2} d^{-1} from the surface to 1000 m [*Mouw et al.*, 2016].

POC fluxes are aligned in time with the midpoint of deployment. Monthly, depth-binned climatologies are retrieved at each measurement location as the median of data grouped by month and depth bin. These locational climatologies are then aggregated by biogeochemical province, retrieving the median across locations. Uncertainty within each depth bin for a given month is represented as the standard deviation of grouped POC flux estimates and is used to weight each value during further analysis.

Not all provinces contained enough depth or temporal resolution to be considered for further analysis. Of the 39 provinces containing POC flux measurement sites, 23 meet our criteria of (1) a minimum of four discrete measurement depth bins throughout the water column, (2) data in at least two (of four) seasons for at least one measurement depth within 300 m of the depth of export, and (3) S_{fm} retrieved in all four seasons. Seasons are defined as December–February, March–May, June–August, and September–November. For criteria (2), most of the provinces had shallow POC flux data in all four seasons with the exception of SARC, MONS and ARAB, which had data in three seasons and NADR and SPSG, which had data in two seasons. Of the qualifying provinces, only 16 resolved significant fits of POC flux versus depth as described below in section 2.5 and are shown in Figure 1.

For satellite products (NPP, S_{fm}, and z_{eu}), the retrieved SeaWiFS time series at each POC flux location is first interpolated to fill gaps less than 60 days apart using a piecewise cubic Hermite interpolating polynomial, a procedure similar to a spline interpolation except that it restricts predicted values from extending beyond measured amplitudes and prevents oscillations in slope between consecutive data points. Gaps

longer than 60 days are not filled. Climatologies are then constructed at each POC flux location as the median of the interpolated time series grouped by month. Monthly satellite climatologies at individual locations are combined to form a provincial climatology, again as the median value of the data set grouped by month.

We perform a sensitivity analysis to assess the difference between combining all pixels within the province area versus only aggregating pixels surrounding POC flux locations when retrieving provincial NPP and S_{fm} climatology (data not shown). The difference between whole-area and locational-derived climatological NPP ranges between 8 and 577 mg C m^{-2} d^{-2} with a mean of 100 mg C m^{-2} d^{-2}. The difference in S_{fm} ranges between 0.4% and 4.9% with a mean of 2.0%. In both cases, the provinces showing the largest difference are GUIA followed by SARC. We repeat the POC flux versus depth analysis as described in section 2.5 below using whole-area NPP and S_{fm} climatology and find no difference in retrieved parameters characterizing POC flux versus depth for any province with the exception of GUIA and SARC. Given the poor spatial coverage of POC flux measurements within each province and the insignificant differences between NPP, S_{fm} and retrieved coefficients from whole-area versus location-based climatologies, we utilize location-based climatology results throughout the rest of our analysis since they better represent the ecological processes directly influencing observed POC flux.

The MLD product is already a monthly climatology. For biogeochemical provinces, MLDs at individual locations are combined to form a provincial climatology as the median value of the dataset grouped by month. The depth of export (z_e, m) is defined as the deeper of either climatological MLD or z_{eu} [*Lutz et al.*, 2007; *Lam et al.*, 2011].

It is common practice to temporally align POC flux at depth with NPP in the surface ocean by accounting for particulate settling velocity. Some studies assume a nominal sinking rate of 70 m d^{-1} or 100 m d^{-1} [e.g., *Dunne et al.*, 2005; *Helmke et al.*, 2010; *Lutz et al.*, 2007]. Others utilize a variety of methods to quantify sinking rate including the "benchmark" method of visually matching event peaks between sediment traps [e.g., *Honjo et al.*, 1995, 2008], cross correlation of a time series between two traps [*Timothy et al.*, 2013; *Muller-Karger et al.*, 2004], or the Fourier fit method of *Xue and Armstrong* [2009]. In practice, these methods assess the shift in time between two signal shapes. The maximum detectable sinking rate is then bounded by the minimum detectable shift in time between two traps, which, in turn, is ultimately determined by the resolution of sediment trap cup intervals [*Armstrong et al.*, 2009; *Xue and Armstrong*, 2009]. In our case, we have combined data into monthly climatologies; thus, the minimum signal shift we can detect is 30 days. If we take an example set of traps that are spaced 1000 m apart and shift them one or two points in time, the maximum detectable sinking rate is 33 m d^{-1} or 16 m d^{-1}, respectively. Although sinking rate estimates vary widely throughout the global ocean, the majority fall between 100 m d^{-1} and 300 m d^{-1}, well above our nominal detection limit (see *Berelson* [2002] and *Xue and Armstrong* [2009] for summary discussions). Thus, we analyze climatological POC flux versus depth in relation to surface NPP and S_{fm} trends without shifting data in time.

2.3. Time Series Sites

Four long-term oceanographic time series locations are explored in a separate analysis of the relationship of POC to export and remineralization: the Carbon Retention In A Colored Ocean (CARIACO) project site in the Cariaco Basin (10.5°N, 64.7°W), K2 in the northwest Pacific (47°N, 160°E), and Ocean Station Papa (50°N, 145°W). The final time series is formed by combining data from the Bermuda Atlantic Time Series (BATS) study site in the Sargasso Sea (31.7°N, 64.2°W) with the Ocean Flux Program (OFP, 31.8°N, 64.2°W). Combining these datasets creates a complete water column profile with BATS sediment traps deployed $\leq$300 m and OFP traps deployed $\geq$500 m. Retrieved NPP and S_{fm} show $<$1% variability between these two locations over the SeaWiFS record, and we elect to analyze the satellite data products from BATS coordinates. All time series locations meet the following criteria: (1) a minimum of four discrete measurement depths throughout the water column, (2) at least one measurement depth within 300 m of the depth of export, (3) data collected throughout at least one continuous year, and (4) S_{fm} retrieved in all four seasons. Unfortunately, the Hawaii Ocean Time series (HOT, 22.8°N, 158.0°W) could not be included here since POC flux is reported at a single depth.

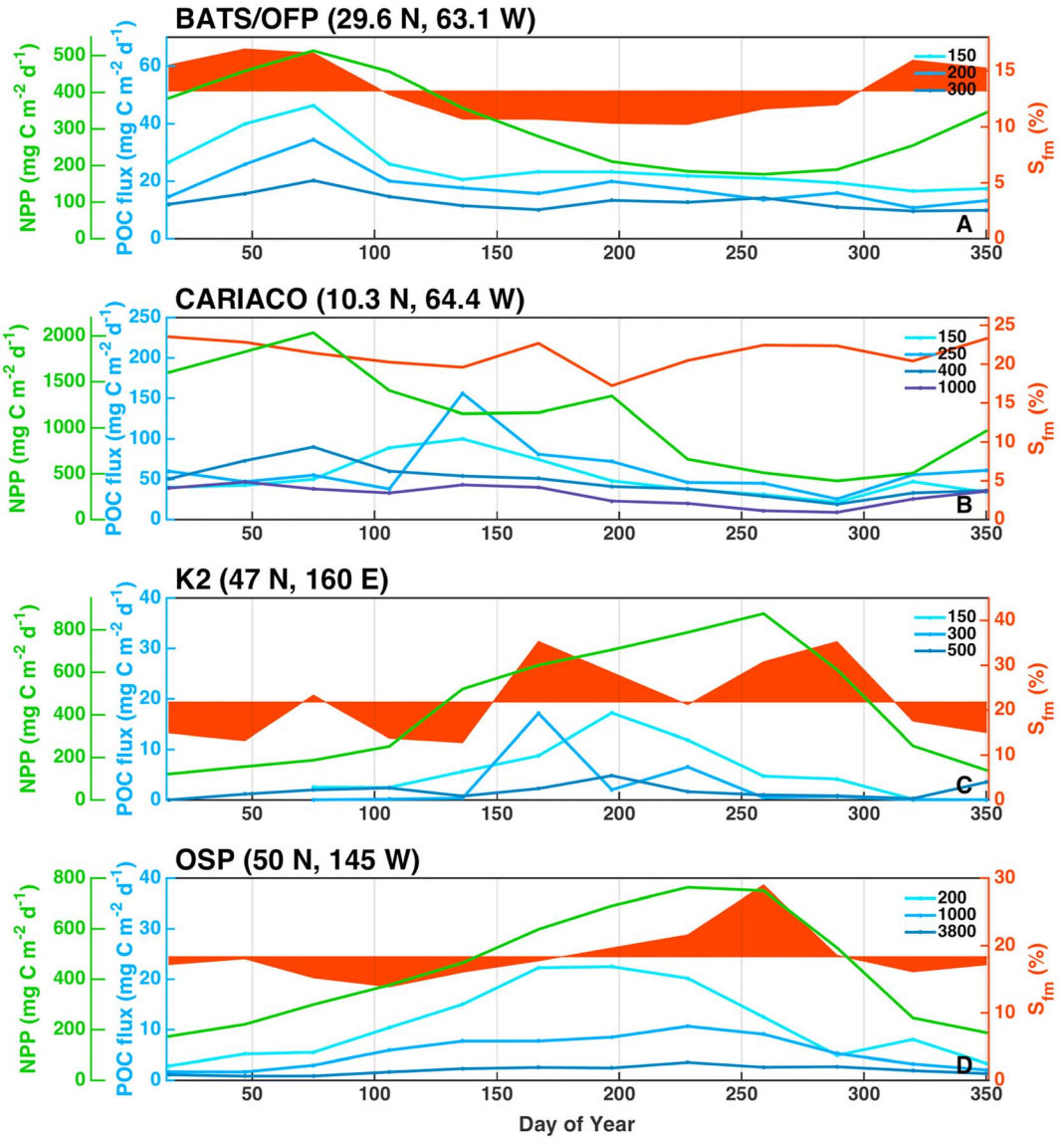

Figure 2. Climatological net primary production (NPP, green), percent microplankton (S_{fm}, orange), and POC flux (blues for depths indicated in the legend) for the time series sites. Times of large and small dominated phytoplankton cell size are shaded. CARIACO did not have a great enough variance in phytoplankton size structure to discriminate between large and small dominance. The horizontal line in S_{fm} indicates the threshold (mean of monthly climatology) used to separate microplankton (above the line) and picoplankton (below the line) dominance. Note different *y* axis scales for each subplot.

2.4. Defining Ecosystem State

To determine the impact of community size structure on POC flux, monthly climatologies are split into times dominated by large or small cells. However, some provinces show very little variability in S_{fm} throughout the year (e.g., Figure 2b) demonstrating shifts in community size structure cannot be detected. To determine which climatologies show detectable changes in ecosystem state, we define the ratio of variance/range (V/R) as a metric of S_{fm} variability. We retrieve V/R for S_{fm} over the SeaWiFS time series for all Longhurst provinces regardless of whether they contain POC flux locations (data not shown). Provinces with V/R greater than the global median (0.32) are split into times when large or small cells dominate; climatologies with $V/R < 0.32$ are only considered as a whole. Of the 16 provinces shown in Figure 1, six qualify for a size-dependent analysis ($V/R > 0.32$): SARC, NADR, NASW, BERS, PSAW, and PSAE. Of the time series locations, BATS/OFP, K2, and OSP all qualify for a size-dependent analysis, while CARIACO showed little change in S_{fm} throughout the climatological year (Figure 2).

For the provinces with detectable changes in community size structure, we perform a sensitivity analysis comparing different thresholds for defining the shift in small-cell versus large-cell dominance. We repeat the analysis of POC flux versus depth described in section 2.5 below for climatologies split by the mean, median, and half the range of S_{fm}. The fit for the large fraction of the BERS province split by half the range of S_{fm} did not converge. Otherwise, confidence intervals on retrieved parameters overlap in all cases (data not shown). Results shown here use the mean of S_{fm} climatology as the threshold of small versus large-cell dominance (Figure 2). We utilize this regional, rather than global, mean of S_{fm} to delineate large and small dominated regimes to assess the impact of local changes in size composition relative to the average ecosystem state.

2.5. Export Flux and Transfer Efficiency

POC flux that sinks beyond the depth of export shows an exponentially decreasing trend with depth. This relationship can be characterized by considering a labile fraction of POC that remineralizes near the export depth and a refractory component that continues to sink through the water column [*Lutz et al.*, 2002]. Prior to fitting, POC flux (F_z, mg C m^{-2} d^{-1}) at each depth is first expressed as a p ratio (p_z, %) by normalizing to surface NPP ($p_z = F_z$/NPP), representing the portion of NPP to reach each depth. The p ratio profiles are expressed as depth below the depth of export (z-z_e) [*Buesseler and Boyd*, 2009] and quantified using the relationship of *Lima et al.* [2014] using a nonlinear least squares procedure:

$$p_{z-z_e} = p_{z_e}\left[\alpha e^{-(z-ze)/\lambda} + (1-\alpha)\right] \quad (1)$$

where p_{ze} is the p ratio at the depth of export, called export efficiency, α is the labile fraction of exported POC (%), and λ is the remineralization length scale (m). Data points are weighted by the standard deviation of POC flux climatology during the fitting procedure. The *Lima et al.* [2014] parameterization is selected over *Martin et al.* [1987] ($F_z = F_{100}\,(z/100)^{-b}$) due to the ability to parameterize more than a single coefficient (b) indicative of flux attenuation related to the remineralization length scale. The refractory portion of exported POC is retrieved as $1-\alpha$ (%). Note that $1-\alpha$ is not a p ratio; it represents the percentage of exported POC, not surface NPP, which reaches the deep ocean and has the potential for sedimentation.

While it would be preferable to retrieve p_{ze}, α, and λ for each month in the climatology, an insufficient number of fits converge to allow for a meaningful seasonal analysis (data not shown). Instead, fitted parameters are retrieved for both time series locations and biogeochemical provinces pooled over the entire climatology or for times when large versus small cells dominate as described in section 2.4. Results are only included where confidence intervals on retrieved parameters do not overlap zero. Five of the six qualifying provinces retrieved fits for both large and small profiles (SARC, NASW, BERS, PSAW, and PSAE); retrievals for NADR did not converge. Absolute export flux (F_{ze}, mg C m^{-2} yr^{-1}) is retrieved as NPP $\times\, p_{ze}$, for NPP integrated over the entire year or for times of small and large dominance.

Transfer efficiency ($TE_{z\text{-}ze}$) represents the fraction of exported organic matter that reaches a given depth below the depth of export ($z - z_e = 100$ m was used here). Transfer efficiency is estimated from fitted results as the retrieved p ratio 100 m below the depth of export (p_{100}) to p_{ze} [*Buesseler and Boyd*, 2009]:

$$TE_{z-z_e} = \frac{p_{z-z_e}}{p_{z_e}} \quad (2)$$

We explore the impact of phytoplankton size composition on the relationship between the p_{ze}, λ, $1-\alpha$, F_{ze}, and TE_{100} at time series locations and between biogeochemical provinces.

3. Results

3.1. Time Series

The four time series locations contrast in the physical, chemical, and biological drivers controlling production and transfer of organic carbon from the surface to the deep ocean. Climatological trends in NPP, S_{fm}, and measured POC flux highlight these differences (Figure 2). Net climatological NPP was highest at CARIACO (410 mg C m^{-2} yr^{-1}), followed by K2 and OSP (both 160 mg C m^{-2} yr^{-1}) and BATS/OFP (115 mg C m^{-2} yr^{-1}). The mean contribution of microplankton to each time series site increases from

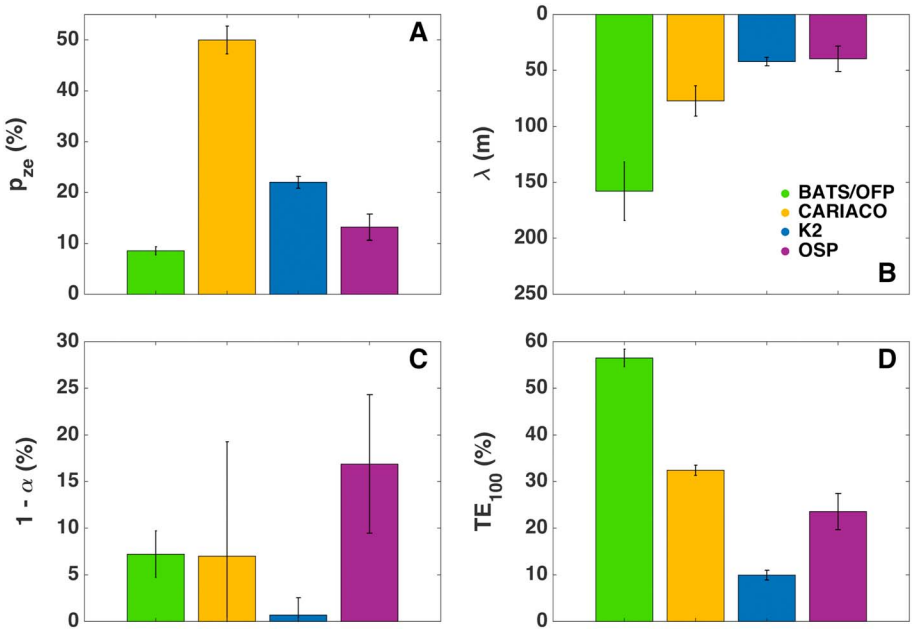

Figure 3. Coefficients for (a) export efficiency (p_{ze}), (b) remineralization length scale (λ), (c) the refractory fraction of exported material ($1-\alpha$), and (d) transfer efficiency 100 m below the depth of export (TE_{100}) for annual results from the time series locations. Results for p_{ze} and TE_{100} are significantly different between all locations. Results for λ are not significantly different between K2 and OSP. The refractory fraction ($1-\alpha$) is not different between any of the locations.

BATS/OFP (13 ± 3%, SD) to OSP (18 ± 4%) to CARIACO (21 ± 2%) to K2 (22 ± 9%) (Figure 2). K2 showed the greatest variability in S_{fm} throughout the year (Figure 2).

When comparing results between locations as a whole, there are marked differences in the efficiency of carbon export and remineralization. Export efficiencies vary between time series sites consistent with greater export in regions of greater production [*Eppley and Peterson*, 1979; *François et al.*, 2002]; p_{ze} is 9%, 50%, 22%, and 13% at BATS/OFP, CARIACO, K2, and OSP, respectively (Figure 3a). However, the dynamics of remineralization and transport to the deep ocean are more nuanced. Just below the depth of export, material at K2 and OSP is more labile than at BATS/OFP and CARIACO as reflected in shallower λ and corresponding lower TE_{100} (Figures 3b and 3d). The proportion of exported material reaching the deep ocean showed no significant difference between the four locations, with $1-\alpha$ averaging 8% (Figure 3c). We hypothesize the differences between sites are related to phytoplankton composition and food web structure.

Given the limited number of locations ($n=4$), broad generalizations regarding the relationship between retrieved parameters and S_{fm} are challenging to quantify (Figure 4). However, time series results also represent the most comprehensive characterization of POC flux versus depth available in the oceanographic community. Trends observed for these distinct ecosystems are repeated in the provincial global analysis (compare Figures 4 and 8). Across time series locations, p_{ze} increases with increasing S_{fm}. However, even through the mean size distribution at CARIACO and K2 are similar, CARIACO has much greater annual p_{ze} (Figure 4a). Remineralization length scale also tends to decrease with increasing size (Figure 4b), although λ is nearly identical at K2 and OSP despite a larger contribution from microplankton at K2. With the exception of CARIACO, which had a high p_{ze} compared to the other locations, greater transfer efficiencies were associated with lower export flux efficiencies (Figure 4c). Also, the p ratio at 100 m below the depth of export (the proportion of NPP to reach $z-z_e=100$ m) was consistently below 5% for all locations (lines in Figure 4c), again with the exception of CARIACO at 16%. Overall, the absolute magnitude of export flux (F_{ze}) showed a strong positive trend with export flux efficiency for annual retrievals (Figure 4d). CARIACO is the most coastally influenced of locations and generally represents an outlier to trends observed at time series sites and throughout the global ocean.

CARIACO is part of the GUIA province, which does not fall above the $V/R > 0.32$ threshold for splitting by size. It is the only time series site that does not demonstrate variability in S_{fm} throughout the year (Figure 2b). Thus,

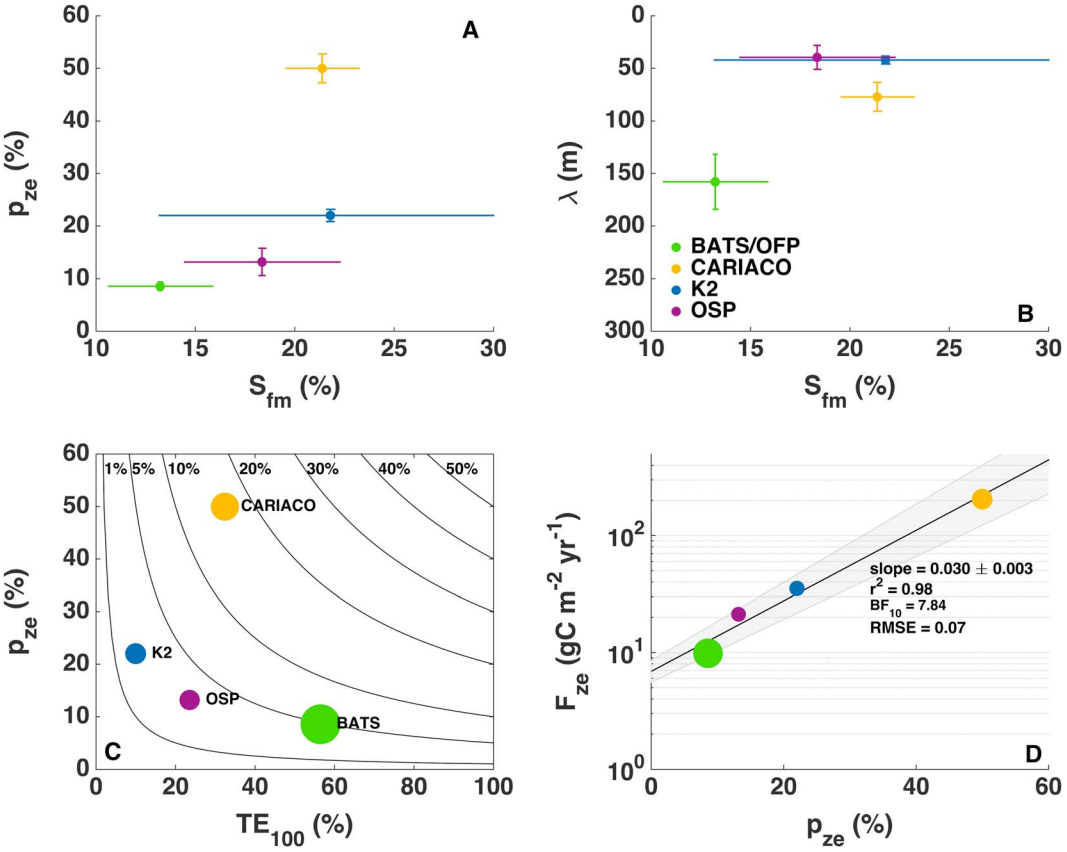

Figure 4. Relationships between (a) export efficiency (p_{ze}) versus mean percent microplankton (S_{fm}), (b) remineralization length scale (λ) versus S_{fm}, (c) transfer efficiency to 100 m below the depth of export (TE_{100}) versus p_{ze}, and (d) absolute POC flux magnitude (F_{ze}) versus p_{ze} for time series locations. The shaded region in Figure 4d indicates the 95% confidence interval of the regression. Size of the markers in Figures 4c and 4d are proportional to λ. Increases in microplankton fraction were associated with higher export efficiency, shallower remineralization length scale, and lower transfer efficiency. Absolute POC flux at the depth of export was significantly correlated with export efficiency.

BATS/OFP, K2, and OSP are split by large and small dominated periods (Figure 2). Export efficiency from climatologies split into large/small periods does not follow the same trend with S_{fm} as seen for annual relationships. While BATS/OFP can be split by size, fitted parameters are not different between large and small dominated periods (Figures 5a–5f). At K2 and OSP, p_{ze} is higher during small dominated periods by 9% and 5%, respectively (Figures 5h and 5n). However, this higher efficiency does not always correspond with a greater absolute flux; error bars for F_{ze} at K2 overlapped between small and large dominated periods while small regimes at OSP are higher by 4 mg C m^{-2} yr^{-1} (Figures 5l and 5r). Like annual results, remineralization length scale is deeper at K2 and OSP for periods dominated by small cells, although error bars overlapped for all of the locations. At OSP, the proportion of exported material reaching beyond the mesopelagic was higher during large-cell dominated times by 12%. K2 showed no difference in the refractory fraction between small and large dominated periods (Figure 5k).

3.2. Global Provinces

P_{ze}, λ, $1-\alpha$, and F_{ze} show variability between the 16 provinces for which POC flux parameters are retrieved (Figure 6). Export flux efficiency (p_{ze}) is high in productive coastal systems and increases with latitude (Figure 6a). It is greatest (33%) in GUIA, which is influenced by the Amazon River outflow. In the northern Pacific, p_{ze} shifts from BERS (33%) in the subarctic through PSAW/PSAE (22% and 17%, respectively) and NPPF (8%), as provinces transition between the Bering Sea and the North Pacific Polar Front. Pacific equatorial provinces PNEC and PEQD are both 8%. In the northern Atlantic, p_{ze} again shifts north to south from SARC (16%) to NADR (9%) and NASW (8%). The lowest p_{ze} value (0.5%) is found in the South Atlantic gyre (SATL).

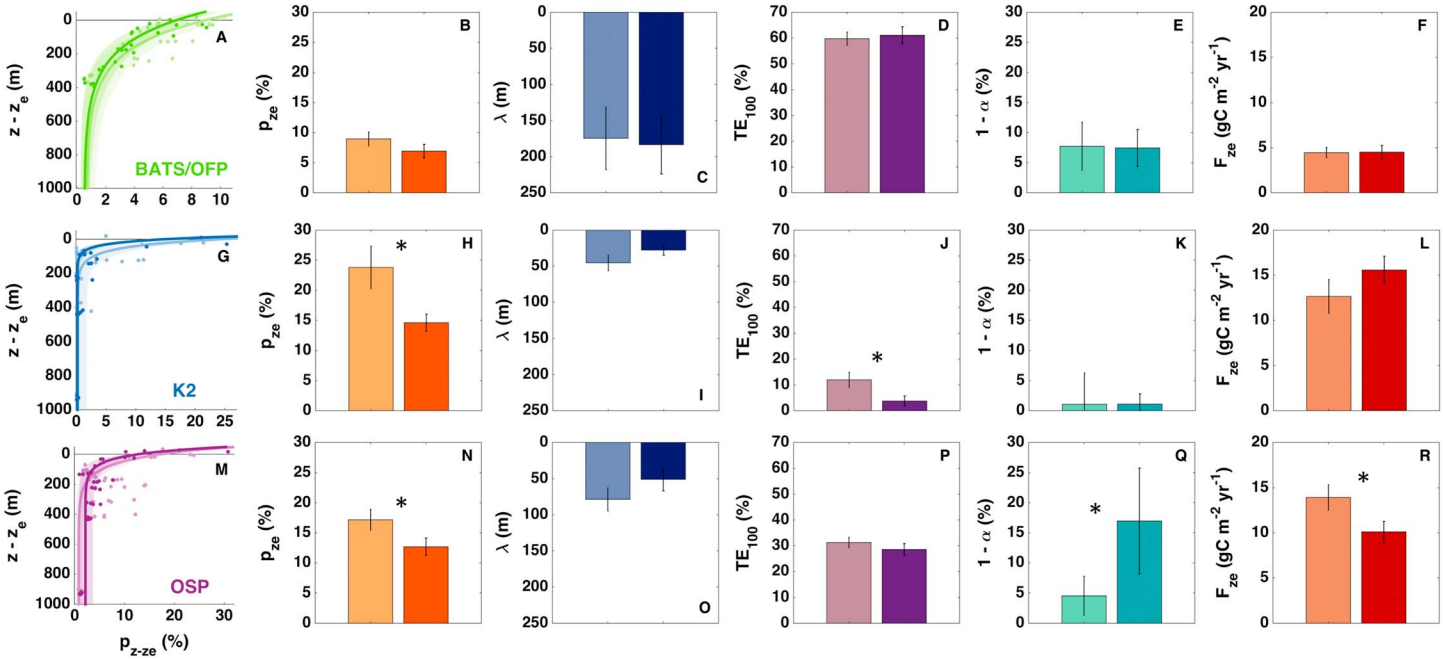

Figure 5. The *p* ratio versus depth below the depth of export pooled by times in the climatology dominated by large and small cells for time series sites fit with equation (1). Results show export efficiency (p_{ze}), remineralization length scale (λ), transfer efficiency to 100 m below the depth of export (TE_{100}), refractory fraction of exported POC ($1-\alpha$), and POC flux at the depth of export (F_{ze}) for (a–f) BATS/OFP, (g–l) K2, and (m–r) OSP. CARIACO did not have a great enough variance in phytoplankton size structure to discriminate between large and small dominance. Lighter and darker shades indicate small and large dominance, respectively. Stars indicate where 95% confidence intervals in retrieved parameters do not overlap.

In general, the subtropical gyres (NADR, NASW, SPSG, NPSW, NADR, and SATL), transitional polar (NPPF), and Indian Ocean (MONS and ARAB) display moderate to low p_{ze} values (4%–10%). In summary, productive ecosystems have greater export efficiency, while oligotrophic ecosystems show low export efficiency [*Henson et al.*, 2012] resulting from local recycling of organic carbon through a tightly coupled microbial loop [*Pomeroy*, 1974].

Remineralization is spatially more variable (Figure 6b). The shallowest length scales (λ) (11 m–61 m) are found in Amazon River influenced (GUIA), North Pacific high-latitude provinces (BERS, PSAW, PSAE), and South Atlantic subtropical gyre (SATL). Deepest λ (307 m–495 m) are found in the Indian Ocean (ARAB and MONS), the Pacific equatorial provinces (PNEC and PEQD), and in the South Pacific subtropical gyre (SPSG). Intermediate λ (154 m–291 m) are found in the interface between the North Pacific subtropical and subpolar gyres (NPPF), the western province of the North Pacific subtropical gyre (NPSW), and throughout the North Atlantic (SARC, NADR, and NASW) (Figure 6b). As a generalization, in the Pacific Ocean, λ is shallow at high latitudes and deepens toward transitional provinces between the subtropical and subpolar gyres. Deepest λ are observed at gyre interfaces and in provinces influenced by equatorial upwelling. Gyre provinces tend to have intermediate to deep λ in both the Pacific (NPSW, and SPSG) and Atlantic (NASW). SATL is the exception with a very shallow λ (11 m). In the Indian Ocean, the coastal and monsoonal provinces both have deep λ (336 and 495 m, respectively).

In addition to p_{ze} and λ, the labile (α) and subsequent refractory ($1-\alpha$) fractions of POC flux are estimated. The latter represents the proportion of exported POC reaching the deep ocean and the potential for sedimentation (Figure 6c). The greatest $1-\alpha$ (82%) is found in the South Atlantic subtropical gyre (SATL). The median *p* ratio for depths greater than 3000 m at SATL is 0.4%, very close to the export efficiency (p_{ze}) of 0.5%. Thus, the refractory portion of exported POC is very high. The next highest $1-\alpha$ are found in the Indian Ocean (MONS and ARAB, 22–23%) followed by the North Pacific subtropical gyre (NPSW, 20%). All other provinces have a refractory fraction of less than 10%.

The magnitude of POC flux at the depth of export (F_{ze}) is helpful to consider when assessing the spatial variability of annual POC flux magnitude (Figure 6d). Generally, higher F_{ze} are found in regions known for higher primary production. The greatest F_{ze} is found in GUIA (134 mg C m^{-2} d^{-1}), which is highly influenced by the

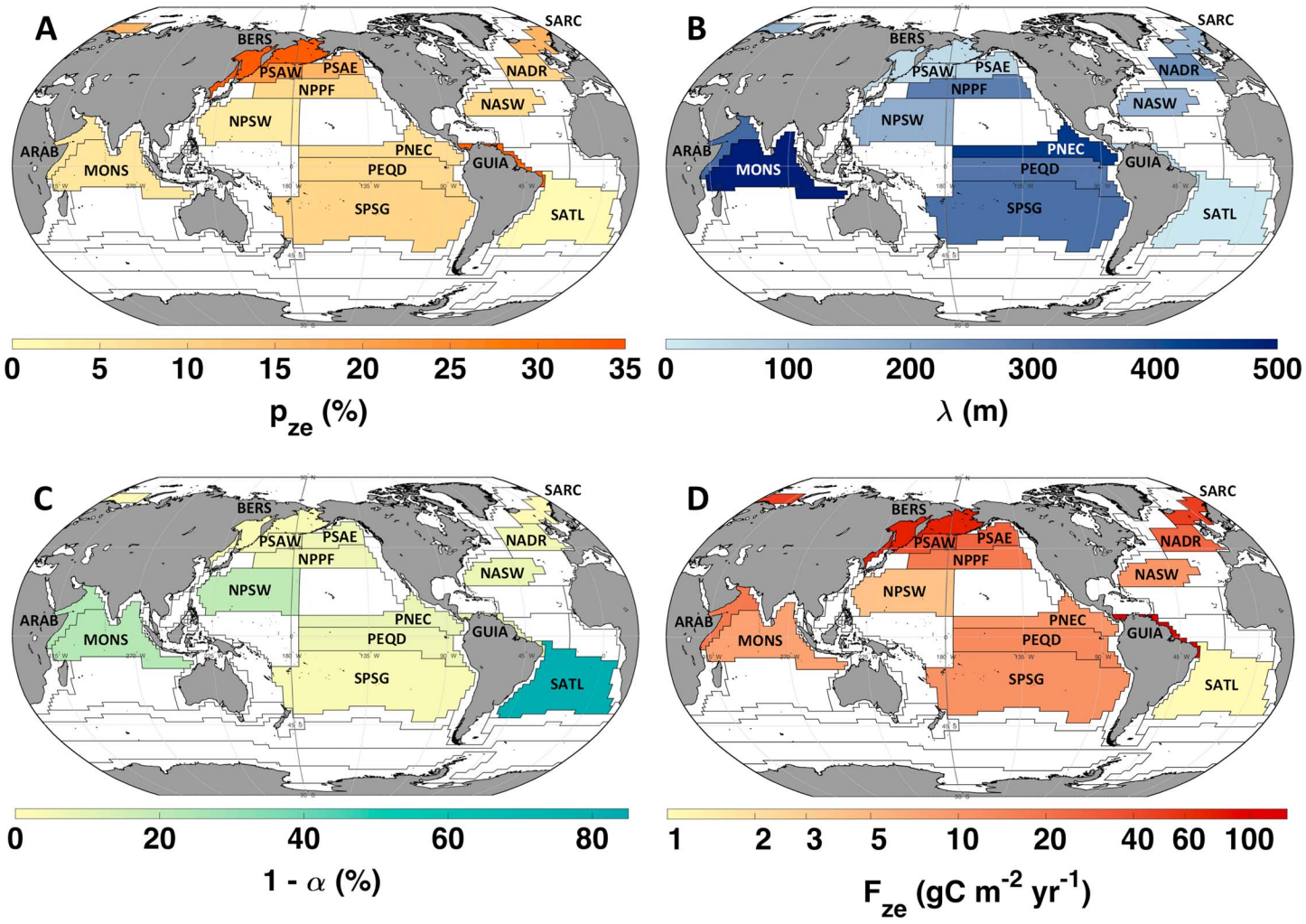

Figure 6. Maps of (a) export flux efficiency (p_{ze}), (b) remineralization length scale (λ), (c) refractory fraction of exported POC ($1-\alpha$), and (d) POC flux at the depth of export (F_{ze}) for provinces with robust fits with equation (1).

Amazon River outflow (Figure 6d). The next highest F_{ze} is found in high-latitude provinces in the Northern Hemisphere: BERS and SARC (72 and 49 mg C m^{-2} d^{-1}, respectively) followed by PSAW, PASE, and NADR that range between 24 and 34 mg C m^{-2} d^{-1}. The Northern Indian Ocean (ARAB) and transitional province between the North Pacific subtropical and polar regions (NPFF) have F_{ze} of 17 mg C m^{-2} d^{-1}. Low F_{ze}, between 4 and 13 mg C m^{-2} d^{-1}, are found in the subtropical gyres of all oceans (NPSW, SPSG, NASW, and MONS) and the equatorial Pacific (PNEC and PEQD). The lowest F_{ze} of 0.4 mg C m^{-2} d^{-1} is in SATL, resulting from a very shallow remineralization length scale and low export efficiency.

Six provinces met the criteria ($V/R > 0.32$) for separation into periods dominated by large and small cells. Five are able to resolve fits with equation (1): BERS, NASW, PSAE, PSAW, and SARC; fits for NADR did not converge (Figure 7). Of these, BERS, NASW, and PSAE had lower export flux efficiency (p_{ze}) during times dominated by large cells. SARC showed the opposite trend (Figure 7a). Remineralization length scale (λ) is consistently deeper for periods dominated by large cells, though error bars overlap for NASW and SARC. Retrieved refractory fraction ($1-\alpha$) is not different between size-dominated periods for any of the provinces. The inability to separate $1-\alpha$ is not surprising as POC flux is most variable in the upper 500 m of the water column, and $1-\alpha$ is dependent on data at depth. POC flux at the depth of export (F_{ze}) is generally larger for periods dominated by large cells, with the exception of PSAE.

By considering p_{ze} and λ together with transfer efficiency 100 m below the depth of export (TE_{100}), we seek to understand the relationship between surface processes and phytoplankton community composition that set

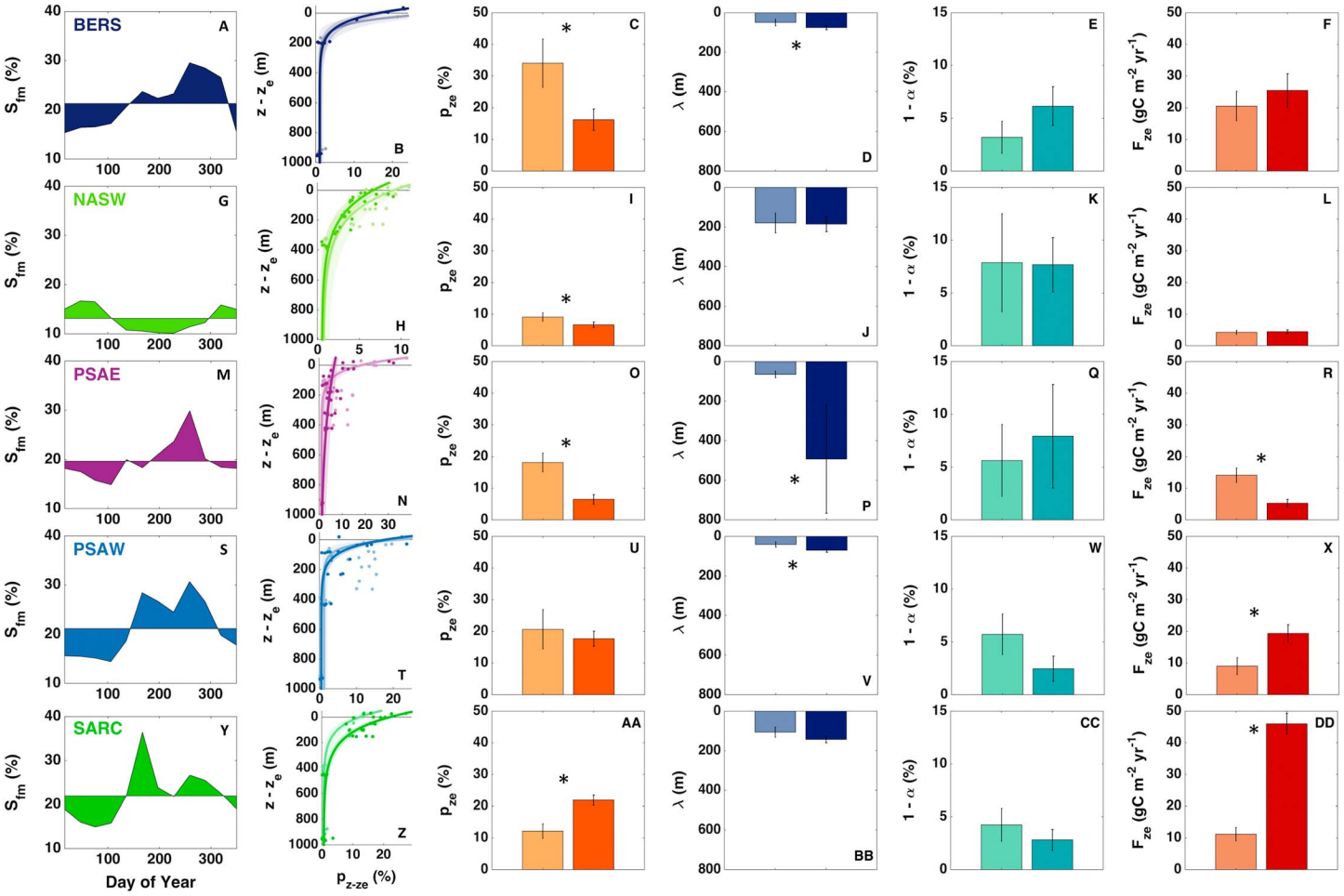

Figure 7. Percent microplankton (S_{fm}) climatology and p ratio versus depth below the depth of export for the five provinces where fits with equation (1) could be resolved with statistical confidence for times of the year split into large and small dominance. Bar graphs show export efficiency (p_{ze}), remineralization length scale (λ), the refractory fraction of exported POC ($1-\alpha$), and POC flux at the depth of export (F_{ze}) for (a–f) BERS, (g–l) NASW, (m–r) PSAE, (s–x) PSAW, and (y–dd) SARC. Lighter and darker shades indicate small and large dominance, respectively. Stars indicate where 95% confidence intervals on retrieved parameters do not overlap.

the strength (p_{ze}) and efficiency (TE_{100}) of the biological pump, and how λ is related to both. For Figure 8a, we follow *Buesseler and Boyd* [2009] by plotting p_{ze} against TE_{100} and with λ expressed as the size of the marker and the mean S_{fm} as the color of the marker. Contour lines indicate the p ratio 100 m below the depth of export (p_{100}). Greater strength and efficiency of the biological pump are characterized by higher p_{ze} and TE_{100} values. Across all provinces, climatological data fall at or under the 10% contour (Figure 8a), indicating that less than 10% of NPP typically reaches 100 m below the depth of export. Generally, regions with a greater proportion of larger cells had higher F_{ze} and p_{ze}, lower TE_{100} and shallower λ (Figures 8a and 8b). When parsing the climatology by periods of time dominated by large and small cells, in all provinces TE_{100} and λ were higher and p_{ze} was lower for large-cell dominated periods (Figure 8c). Additionally, F_{ze} was higher for large dominated periods in all provinces except PSAE (Figure 8d).

We consider each of the fitted parameters from equation (1) as they relate to S_{fm} using type II linear regression for either standard (p_{ze} and λ) or log transformed ($1-\alpha$ and F_{ze}) data. Bayes factors (BF_{10}, unitless) are retrieved to assess fit significance [*Wetzels and Wagenmakers*, 2012]. Briefly, Bayes factors represent the likelihood that data occur under one model versus another. In the case of linear regression, BF_{10} compares the ratio of the likelihood that a slope should be included in the model (slope = nonzero) versus that it should not (slope = 0). Bayes factors can be interpreted literally, so that $BF_{10} = 2$ means the data are 2 times more likely to be explained by including a nonzero slope in the model versus not. Thus, $BF_{10} > 1$ provide evidence the retrieved slope is significant, while $BF_{10} < 0$ indicate that the slope is 0. Both F_{ze} and p_{ze} increase along with

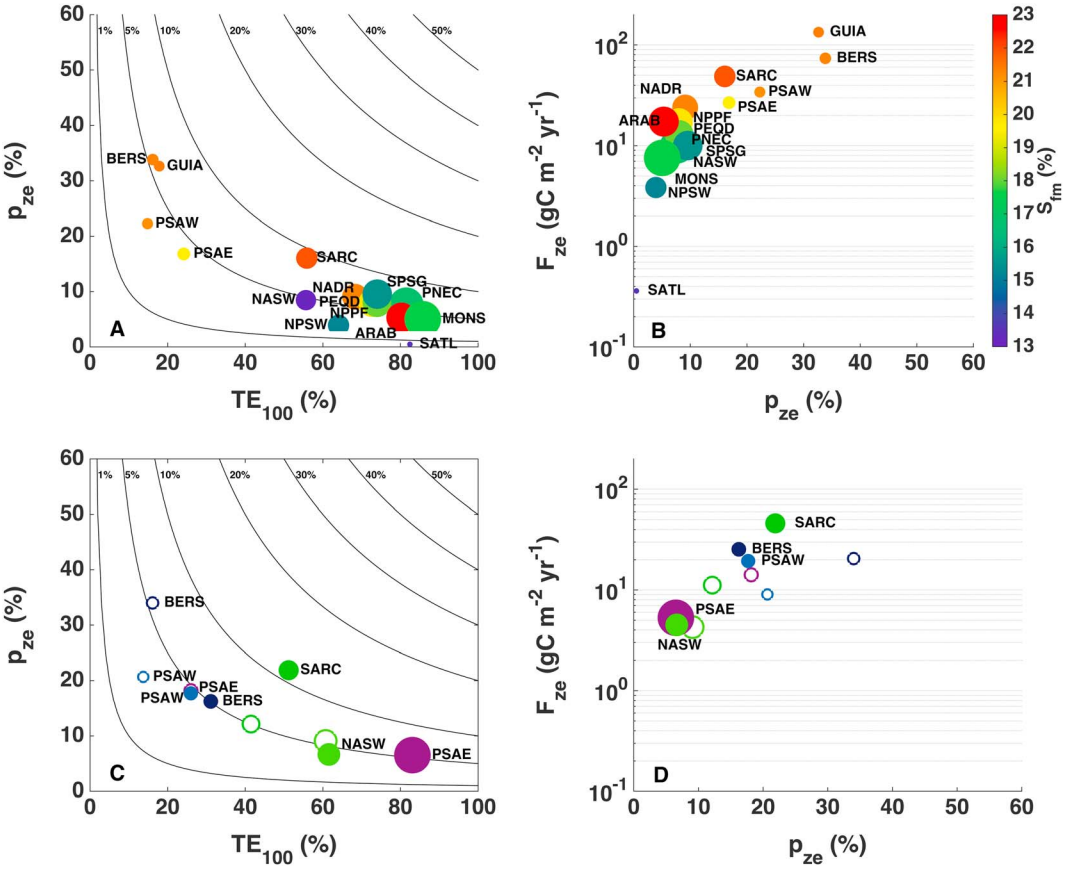

Figure 8. Export flux efficiency at the depth of export (p_{ze}) versus transfer efficiency 100 m below the depth of export (TE_{100}) for (a) whole provinces and (c) provinces split by large and small dominated periods. Contour lines indicate the p ratio 100 m below the depth of export (p_{100}). These figures represent the strength and efficiency of the biological pump, where the upper right hand corner of each subplot would be the most efficient. The size of the marker is proportional to remineralization length scale (λ) and the color of the marker represents the percent microplankton (S_{fm}) (Figure 8a) or province (Figure 8c). POC flux at the depth of export (F_{ze}) versus p_{ze} for (b) whole provinces and (d) provinces split by large and small dominance. Marker size and color as in Figures 8a and 8c. Open and closed circles in Figures 8c and 8d represent small and large dominated periods, respectively.

S_{fm} (Figures 9a and 9d), suggesting that both the magnitude and efficiency of export flux increases as larger cells make up a greater portion of the community. The relationship with F_{ze} is particularly strong with $BF_{10} = 64$. On the other hand, $1 - \alpha$ decreases with increasing S_{fm} (Figure 9b), suggesting that once exported, POC from large-cell regimes is more labile within the twilight zone. Although retrieved slope for λ versus S_{fm} indicates a shallowing of the remineralization length scale with increasing S_{fm}, that $BF_{10} = 0.2$ indicates the slope was not significant.

4. Discussion

4.1. Time Series Sites

Differences in export flux efficiency and remineralization between oceanographic time series locations can be related to a combination of phytoplankton size structure, species composition, and local food web dynamics. When comparing between time series locations, and thus different ecosystems, p_{ze} is positively correlated with both S_{fm} and F_{ze} (Figure 4). However, despite almost identical mean annual S_{fm} of 21% and 22% at CARIACO and K2, respectively, the export and remineralization of POC is markedly different between the two locations (Figure 3). The phytoplankton assemblage at CARIACO is diverse and varies in association with El Niño–Southern Oscillation (ENSO) events that correspond with the introduction of pelagic plankton into the coastal species community [*Montes et al.*, 2012; *Pinckney et al.*, 2015; *Romero et al.*, 2009]. The majority of primary

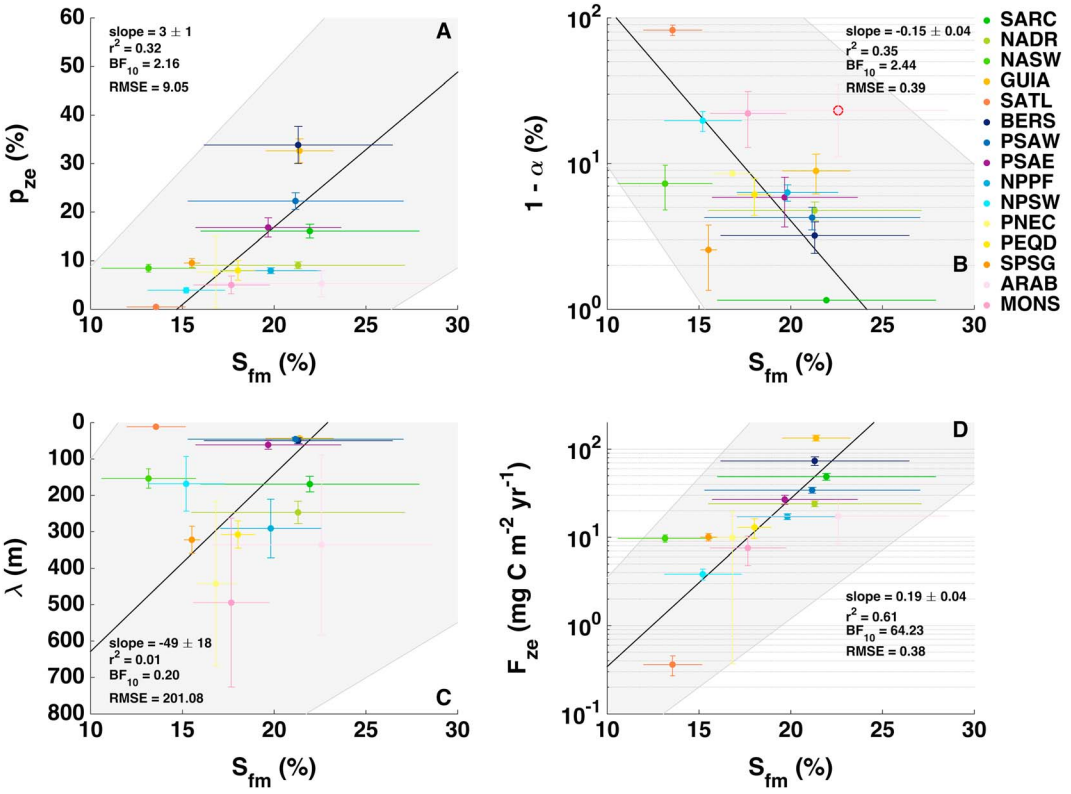

Figure 9. Relationships between mean percent microplankton (S_{fm}) and (a) export flux efficiency (p_{ze}), (b) refractory fraction ($1-\alpha$), (c) remineralization length scale (λ), and (d) POC flux at the depth of export (F_{ze}) for fitted provinces. Provinces are colored as in Figure 1. Regressions are Type II with data circled in red excluded as outliers. Shaded regions represent the 95% confidence interval of the regression fit. Increases in microplankton fraction were associated with greater export efficiency, lower refractory fractions, and greater absolute exported POC.

production occurs close to the surface (<50 m), and most remineralization takes place above the depth of anoxia at 250 m [*Montes et al*., 2012]. Our annual results are consistent with these observations: median climatological z_e (80 ± 10 m, SD) plus retrieved λ (77 ± 14 m, 95% confidence interval) is well above the 250 m anoxic horizon. Our estimate of p_{ze} (50%, Figure 3a) for CARIACO is slightly higher than those reported in *Thunell et al*. [2007] and *Montes et al*. [2012] of up to 44%, although error estimates between data shown here and literature results would overlap. Export flux efficiency at CARIACO has been directly related to ballasting materials, such as opal and calcium carbonate from diatoms, foraminifera, and coccolithophores [*Montes et al*., 2012], rather than aggregation through higher trophic levels, although regional dynamics may be shifting in response to changes in trade wind intensity [*Pinckney et al*., 2015]. This is in direct contrast to K2 in the Western Subarctic Gyre of the Pacific Ocean, which has an active migrating zooplankton community [*Buesseler et al*., 2008] and where large-celled diatom species (upward of 80 μm) dominate the phytoplankton community even during nonbloom periods resulting in some of the highest observed POC:PIC in the world [*Buesseler et al*., 2008; *Honda*, 2003; *Honda et al*., 2006, 2015]. Thus, while export flux efficiency at K2 is still relatively high (22%) when compared to BATS/OFP (Figure 3) or small-cell dominated global provinces (Figure 6), it is low when compared with CARIACO (50%), consistent with recycling through higher trophic levels in the surface layer. This suggests local phytoplankton community composition and grazer dynamics, in addition to overall size structure, play a role in controlling POC export and contribute to variability observed in p_{ze} versus S_{fm} (Figures 4 and 9). In the literature, export flux ratios reported for K2 on event-scale timeframes range from 11 to 21% [*Buesseler et al*., 2008], to 31% [*Honda et al*., 2015], to 17–46% with an annual mean of 29% [*Kawakami and Honda*, 2007]. Our estimate for annual p_{ze} at K2 falls within this range (Figure 3). The active transport of material by diel zooplankton migration translates into a loss of POC near the depth of export [*Buesseler et al*., 2008], shallowing λ and decreasing T_{100} as also seen in our results (Figures 4b and 4c): ~90% of exported material at K2 is lost in the first 100 m below the depth of export compared with ~68% for CARIACO.

The phytoplankton community at OSP had a mean S_{fm} of 18%, lower than both K2 and CARIACO (Figure 2), although net annual production is almost identical to K2. OSP is located in the northeast Pacific Ocean in the southern part of the Alaska Gyre in a high-nutrient low-chlorophyll (HNLC) region that is iron limited [*Mackinson et al*., 2015; *Timothy et al*., 2013; *Wong et al*., 1999]. Diatoms, coccolithophores, and foraminifera contribute significantly to POC flux at OSP, although there is a large interannual variability in species composition related to ENSO events [*Timothy et al*., 2013; *Wong et al*., 1999]. The ratio of PIC to biogenic silica in middepth sediment traps ranges between 1.0 and 1.5 throughout the year [*Wong et al*., 1999] placing equal importance on these two ballasting materials, in contrast to K2, which is dominated by silica. Export flux efficiency at OSP was 13%, midway between BATS/OFP and K2 (Figure 3a). This value is lower than *f* ratios for the region (27–36%) [*Timothy et al*., 2013], but higher than the export flux efficiency of 3.1% reported by *Timothy et al*. [2013] using traps at 200 m. The authors propose that this discrepancy was due to the mismatch of actual export depth versus sediment trap deployment at a consistent 200 m. For our data set, mean z_e was 81 ± 10 m (SD), which is ~100 m above the 200 m trap throughout the year. Thus, we retrieve p_{100}, the fitted ratio of POC flux to NPP at 100 m below the depth of export, which should be equivalent to the export flux ratio reported by *Timothy et al*. [2013] for the 200 m trap deployment. Our p_{100} was 3%, indicating agreement. This example underscores the importance of accurate POC flux measurements close to the depth of export for the retrieval of p_{ze} as labile material is quickly lost when transfer efficiency is low. It also highlights the importance of retrieving p_{ze} from a water column profile rather than a single discrete measurement depth: an important consideration when planning future field campaign efforts. The remineralization length scale at OSP overlaps that of K2 (Figure 3c), although transfer efficiency is more than double (24% at OSP versus 10% at K2). This is consistent with grazer dynamics at K2 as well as other literature suggesting siliceous ballasting material is more labile than carbonate [*François et al*., 2002].

At the other end of the spectrum, BATS/OFP is dominated by picoplankton and nanoplankton throughout the year and the location had the lowest annual S_{fm} of the time series sites (Figure 2) [*Brew et al*., 2009; *Helmke et al*., 2010; *Krause et al*., 2009]. Export flux efficiency at BATS/OFP was 9% ± 1%, the lowest of the time series locations. This result agrees well with annual export efficiencies reported in *Lomas et al*. [2013] of 5–10%. Remineralization length scale is the deepest of all time series locations by at least a factor of 2 at 158 ± 26 m (Figure 3b), which translates into a high transfer efficiency of 56% (Figure 3d). Thus, while 90% of material at BATS/OFP is either respired within the surface layer or laterally transported from the site, exported material from these smaller cells is more refractory than other locations as less than half is lost close to the export depth.

While p_{ze} is positively correlated with both S_{fm} and F_{ze} between time series locations (Figure 4), when individual sites are split by large and small, the local response to changes in community size structure was somewhat different (Figure 5). At BATS/OFP, microplankton contribution increases from 10 to 17% from December through March (Figure 2), concurrent with the winter/spring bloom in the North Atlantic Subtropical Gyre [*Lomas et al*., 2013; *McGillicuddy et al*., 1998]. Diatoms and coccolithophorids become more prevalent [*Brew et al*., 2009; *Helmke et al*., 2010; *Krause et al*., 2009], although common species, such as *Minidiscus* sp., are small (<5 μm) [*Lomas et al*., 2009] and would not be classified as microplankton in our retrieval. We see no difference in export or remineralization at BATS/OFP between large and small dominated regimes. This is consistent with *Helmke et al*. [2010], who also found a low seasonal variance of <1% difference in export efficiency at 200 m throughout the year.

At both K2 and OSP, there was a decrease in export flux efficiency at times dominated by microplankton (Figure 5). At K2, p_{ze} shifts from 24% to 15% as microplankton contribution increases along with NPP during summer and fall months (Figure 5). This is accompanied by a shallowing of λ, although error bars overlapped. Ultimately, 1% of exported material reaches the deep ocean regardless of overlying size class. These results are consistent with reported grazer community response to times of high production [*Wilson et al*., 2008]. *Honda et al*. [2015] also report a negative correlation between primary production and the export flux ratio at K2. However, the literature is mixed for this region with other studies reporting increases (17% to 46%) [*Kawakami and Honda*, 2007] and decreases (21% to 11%) [*Buesseler et al*., 2008] in export flux efficiency concurrent with the summer bloom as larger cells become more prominent. OSP also shows a decrease in p_{ze} from 17% to 13% as microplankton become more dominant (Figure 5). While λ also shallows at OSP for larger cells, again error bars overlapped. However, material from microplankton was ultimately more refractory as

$1-\alpha$ was 17% compared with 5% during times dominated by small cells. These values agree well with the estimates *Lampitt and Antia* [1997], who report a *p* ratio at 2000 m of 1.8–2.1% at OSP. In our case, this would be equivalent to $p_{ze} \times (1-\alpha)$, which is 2% when large cells dominate. Our results add weight to the growing body of literature underscoring the importance of picoplankton contribution to POC flux both at time series locations and throughout the ocean in general [*Brew et al*., 2009; *Lomas and Moran*, 2011; *Mackinson et al*., 2015; *Richardson and Jackson*, 2007].

4.2. Global Provinces

Each biogeochemical province has different physical dynamics forcing biological ecosystem structure and function. As such, we would not expect uniform response of export flux across the globe [*Passow and Carlson*, 2012; *Guidi et al*., 2015]. Though it only retrieves a single empirical coefficient representative of remineralization, the *Martin et al*. [1987] equation is widely used. This means there are few studies to which p_{ze}, $1-\alpha$, and F_{ze} could be directly compared. One such study is the modeling efforts of *Lima et al*. [2014], who retrieve p_{ze}, λ, and α throughout the global ocean for annual mean POC flux profiles estimated at individual model grid points. Results from the polar North Pacific, equivalent to the BERS province, are not well resolved by *Lima et al*. [2014] and are excluded from this discussion. Annual export efficiency from *Lima et al*. [2014] showed similar trends to those seen here with p_{ze} increasing with latitude (Figure 6a). The lowest values ($\leq$5%) are reported in the South Atlantic, equivalent to our results for the SATL province ($<$1%). Throughout the rest of the oceans, absolute values of p_{ze} found in *Lima et al*. [2014] are identical to our results for all provinces with three exceptions: the Amazon coastal province (GUIA), where we report a higher p_{ze} of 33% compared to their 9%, and the Indian Ocean provinces (ARAB and MONS), where we report lower p_{ze} of 5% compared to their 9%–15%. Results for $1-\alpha$ are also similar between the two studies, with refractory fractions throughout most of the ocean at or below 20%. The only notable difference is in the South Atlantic (SATL) where we retrieve $1-\alpha = 82\%$, compared with $1-\alpha = 10\%$ for *Lima et al*. [2014]. These differences are potentially related to model parameterization. Throughout the North Subtropical Atlantic, as defined by *Lima et al*. [2014], which would include the GUIA province, their model repeatedly underestimates field measurements of POC flux at shallow depths, consistent with also underestimating p_{ze} compared to what we observe. Their model performs better in the Indian Ocean but tends to slightly overestimate POC flux at shallow depths, again consistent with the discrepancy of higher p_{ze} than retrieved in our study.

Remineralization length scale can be assessed either as λ or as the remineralization coefficient (*b*) of *Martin et al*. [1987]. *Guidi et al*. [2015] estimate *b* for the same Longhurst provinces used here. Likewise, the modeling study of *Henson et al*. [2012] considers global patters in *b* on a finer scale. We discuss trends in remineralization found by *Guidi et al*. [2015] and *Henson et al*. [2012] since *b* and λ cannot be directly compared along with a direct comparison of our results to λ retrieved by *Lima et al*. [2014]. Both *Guidi et al*. [2015] and *Henson et al*. [2012] found lower *b* (equivalent to deeper remineralization) toward the equator, with the deepest remineralization in the southern Indian Ocean. Our results agree well, with the shallowest λ at high latitudes and the deepest λ toward the equator. *Henson et al*. [2012] predict deeper remineralization in the equatorial Pacific than shown for the same region in *Guidi et al*. [2015]; our results agree with the former. There is also some disagreement in SATL where our estimates suggest shallower remineralization than retrieved in either of these two studies (Figure 6b). *Guidi et al*. [2015] retrieve *b* in a greater number of provinces by including Underwater Vision Profiler (UVP) data. The UVP observes particles greater than 100 μm, which includes only chain-forming diatoms or particle aggregates [*Stemmann and Boss*, 2012]. Disagreement in results could be a due to a combination of increased data resolution in near surface observations and the lack of capture of smaller particles with the UVP.

Absolute values for λ from our study agree less strongly with *Lima et al*. [2014] than results for p_{ze} and $1-\alpha$. Remineralization length scale agrees well throughout the North Atlantic (SARC, NADR, and NASW) and in the Northwest Pacific gyre region (NPSW). We retrieve equivalent locations for the deepest λ in the Indian Ocean (ARAB and MONS) and in the Northern Equatorial Pacific (PNEC) as well as for the shallowest λ in the South Atlantic (SATL), although absolute values are different. However, we retrieve deeper λ in the southern Equatorial Pacific (PEQD) and gyre region (SPSG) as well as much shallower λ in the subpolar region (PSAW and PSAE) with differences of up to 200 m. Thus, *Lima et al*. [2014] report a deepening of λ with increasing latitude, which is opposite to the trend we observe in the Pacific (Figure 6b) and to the trends reported in *Guidi et al*. [2015] and *Henson et al*. [2012] although similar to that found in *Marsay et al*. [2015]. *Marsay*

et al. [2015] consider only neutrally buoyant traps deployed in the North Atlantic but extrapolated globally. They conclude that warmer waters found in oligotrophic regions have shallower remineralization depths than cooler higher-latitude regions due to organic material being inherently more labile in warm surface water. They argue that methods utilizing sediment trap data have too much reliance upon deep observations, misrepresenting POC flux attenuation in the upper few hundred meters of the water column. It is important to point out that the neutrally buoyant traps that *Marsay et al*. [2015] utilized had a maximum sampling duration of 96 h, thus capture event-scale processes rather than climatological results reported here. Further, in aiming to consider the most extensive compilation of POC flux estimates across the globe, data from sediment traps outnumber neutrally buoyant traps or any other observational approach. However, the POC flux data set utilized in this study considered as many shallow observations as possible and the fitting criteria of ensuring POC flux observations within 300 m of the depth of export should reduce reliance on deep observations. We agree with *Marsay et al*.'s [2015] assessment that the *Martin et al*. [1987] function is an oversimplification of POC flux attenuation over the whole water column. To help to improve this, equation (1) resolves more parameters than the remineralization coefficient alone, potentially allowing for more targeted discrimination of factors contributing to the POC flux profile.

The *Buesseler and Boyd* [2009] framework for considering export efficiency and transfer efficiency together is helpful in comparing provinces (Figure 8a). It is important to note that *Buesseler and Boyd* [2009] considered event-scale observations; thus, some of their data fall above the 20% p_{100} contour in contrast to climatological results shown here. Generally, λ deepens as POC export becomes less efficient and POC transfer becomes more efficient (i.e., TE_{100} increases and p_{ze} decreases). Low- to middle-latitude provinces show the highest transfer efficiencies and lowest export flux ratios while high latitudes and the Amazon River influenced coastal province (GUIA) have the lowest TE_{100} and greatest p_{ze} (Figure 8a). These general relationships agree with previous findings. High p_{ze} and low TE_{100} at high latitudes suggests sinking material is labile and more prone to remineralization (i.e., shallower λ), while at lower latitudes the small fraction of NPP exported is more refractory (i.e., deeper λ) [*Lam et al*., 2011; *Henson et al*., 2012].

4.3. Impact of Phytoplankton Size

Under the paradigm of high export efficiency and low transfer efficiency at high latitudes and vice versa for low latitudes [*Henson et al*., 2012; *Lam et al*., 2011; *Lima et al*., 2014], one expects low-latitude regions to congregate in the lower right corner of Figures 8a and 8c and high-latitude regions to fall in the upper left. For the most part, this is what we find when considering all data fitted together (Figure 8a). If we further suppose that high latitudes see a greater impact of microplankton compared with low latitudes, we may expect that progressing from small-cell dominated periods to large-cell dominated periods would result in moving from the lower right to the upper left in Figure 8c. Between provinces, this is generally true. However, within a given province over the seasonal cycle, we find the contrary: the greater presence of large cells leads to decreased export efficiency and increased transfer efficiency (Figure 8c). This is likely due to species composition. Larger cells have a greater chance of being associated with ballasting materials; silica and carbonate are less labile and thus result in greater transfer efficiency [*Armstrong et al*., 2009; *Fischer et al*., 2009; *François et al*., 2002; *Klaas and Archer*, 2002].

Lam et al. [2011] hypothesize that community structure determines transfer efficiency where large cells are transferred less efficiently than small cells. They further suggest that two regimes influence the strength and efficiency of the biological pump: (1) low to moderate POC concentrations with constant high transfer efficiency and (2) bloom regime where the peak of the bloom is characterized by a weak biological pump and low transfer efficiency. They move beyond the simplistic idea of high export flux but low transfer efficiency in more productive regions and vice versa for oligotrophic regions and incorporate consideration of seasonal variation. Their effort focused on particles $>53\ \mu m$ from their Multiple Unit Large Volume in situ Filtration System. Ideally, their low POC and bloom regimes could be compared to our small size and large size dominated periods, but their samples fall mostly within the PSAE, PNEC, PEQD, SANT, ANTA, and coastal provinces where our data set showed too little S_{fm} variability to be split by size (PNEC and PEQD), or where there was insufficient seasonal coverage of POC flux observations (SANT and ANTA). In our results, PSAE was the only province in which F_{ze} in large dominated periods (presumably similar to their bloom regime) was less than small dominated periods (Figure 7r), so it is difficult to compare to the regions in which *Lam et al*. [2011] had data. Nevertheless, we do agree with *Lam et al*. [2011] in finding high-latitude provinces with greater S_{fm}

range have lower overall transfer efficiency than lower latitude provinces with low S_{fm} range. We do not find declining transfer efficiency with a greater proportion of large cells in the ecosystem (Figure 8c). The *Lam et al.* [2011] bloom regime is more difficult to compare to in part because all cells >20 μm are considered together in this study rather than those >53 μm sampled by *Lam et al.* [2011] and because event-scale blooms are averaged into monthly climatologies.

Similar to *Guidi et al.* [2009], we find more carbon is exported from the euphotic zone when larger cells dominate. Absolute export flux increases with S_{fm} for the time series sites and all provinces (Figures 4 and 9). When we consider times of the year dominated by small and larger cells, we find that when small cells dominate, a greater proportion of the NPP is exported, but this POC is remineralized close to the depth of export, i.e., transferred less efficiently. When large cells dominate, export efficiency is lower, but the proportion that is exported is generally more refractory and thus sinks faster, leading to greater transfer efficiency (Figure 8) [*Armstrong et al.*, 2009; *Fischer et al.*, 2009; *François et al.*, 2002; *Klaas and Archer*, 2002]. This provides evidence for a different trophic community response to large versus small cells: when larger cells are present, the majority of labile POC is recycled within the euphotic zone, while when smaller cells dominate, labile POC is more likely to be exported and recycled within the "twilight zone."

While considering phytoplankton cell size, we begin to grow our understanding of particle source relationship to export flux. Not surprisingly, phytoplankton size alone does not capture all the variability of the system. Phytoplankton composition, impacting silica, and carbonate fractions of flux, no doubt plays a role. Here we take a broad view of what can be learned about these processes at province scales by focusing just on the size the phytoplankton cell. Looking further into phytoplankton composition could lend further insight. Carbon export is also affected by zooplankton and other components of the food web. *Siegel et al.* [2014] found direct phytoplankton contribution to total export flux was on average only 12.7%, with values greater than 20% found only high-latitude and upwelling regions, leaving a significant portion of the export to be controlled by flux of fecal matter from zooplankton grazing. By partitioning our analysis into provinces, we assume similar food web structures and thus impacts of higher trophic levels on phytoplankton composition, particle aggregation, zooplankton grazing, and feces production. In the natural world, where all processes are aggregated in the resulting POC flux, the absolute impact of phytoplankton alone on export flux is challenging to quantify, but it is clear from this analysis that the absolute magnitude of carbon flux and the efficiency with which it is exported, remineralized, and transferred does have dependency on the size of the phytoplankton cell upon which the ecosystem is acting.

5. Conclusions

Due to rapid remineralization within the first 500 m of the water column, shallow observations are required to capture the impact of phytoplankton size on export flux. Deep sediment traps alone do not reveal these impacts. Depth resolution and/or parameter variability preclude discrimination of interannual, site-specific size impacts. As the community invests in future flux observations, prioritization of shallower observing techniques, while still characterizing full water column profiles, will enable an even more robust understanding of the role phytoplankton composition plays in carbon flux in the ocean.

Within annual climatologies composited in this study, phytoplankton size impacts on absolute export flux magnitude and efficiency, as well as remineralization length scales, are discerned where enough data are present and phytoplankton size composition showed dynamic range over the annual cycle. The paradigm that more carbon is exported with larger cells holds, but when considering the efficiency of this flux, larger cells are not more efficient. Considering all data together, we find the idea of high export flux efficiency and low transfer efficiency in more productive regions and vice versa for oligotrophic region holds. However, when parsing by dominant size class, we find a contrary relationship. Generally, periods dominated by small cells have lower transfer efficiency and greater export flux efficiency than periods when microplankton comprise a greater proportion of the phytoplankton community. When large cells dominate, the portion exported is generally more refractory thus sinks faster, leading to greater transfer efficiency.

As pointed out as an urgent need by *Lam et al.* [2011], this paper connects POC flux measurements with phytoplankton community structure and the length of time each province spends in both size regimes. These findings point to the importance of considering seasonal variability in phytoplankton composition in model frameworks and the need for the export ratio and remineralization length scales to vary in both space and

time based on community composition. This more dynamic and mechanistic view of export will lead to improved model characterization of POC flux in the ocean as demonstrated by *Lima et al*. [2014], who found increased model performance with regionally varying parameterizations of POC export and remineralization. In addition to broad interregional impacts relating to differences in phytoplankton size distribution, our results also support the need for consideration of local, i.e., within province, seasonal changes in POC export efficiency and remineralization directly linked with cell size in future model development [*Lima et al*., 2014].

As the ocean warms, a decline in the spatial extent and temporal occurrence of large cells has been noted [*Rousseaux and Gregg*, 2015]. If a trend to greater spatial and temporal dominance of small cells continues, our results suggest that this may lead to less overall export but that material will be efficiently exported, with the net effect being less POC transferred to the deep ocean. This has potentially significant implications for atmospheric CO_2 drawdown and carbon sequestration in the deep ocean. This effort provides a step toward greater understanding of the impact of phytoplankton size composition on export to improve our current estimates of carbon flux in the ocean as well as enable more robust projections for the future.

Acknowledgments

We would like to thank the Ocean Color Processing Group at NASA GSFC for the processing and distribution of the SeaWiFS imagery (http://oceancolor.gsfc.nasa.gov) and the Ifremer/LOS Mixed Layer Depth Climatology group for retrieval and distribution of MLD estimates (www.ifremer.fr/cerweb/deboyer/mld). The SeaWiFS phytoplankton size composition imagery was provided by C.B. Mouw and is freely available on PANGAEA (doi.pangaea.de/10.1594/PANGAEA.860474). The compilation of POC flux data along with matched satellite data products used in this study are freely available on PANGEA (doi.pangaea.de/10.1594/PANGAEA.855600). We would like to thank Min Wang for guidance with Bayesian statistical techniques. Comments from two anonymous reviews greatly improved the manuscript. The National Aeronautics and Space Administration (NNX11AD59G and NNX13AC34G) provided financial support for this effort. This is contribution number 31 of the Great Lakes Research Center at Michigan Technological University.

References

Abell, R. E., T. Brand, A. C. Dale, G. H. Tilstone, and C. Beveridge (2013), Variability of particulate flux over the Mid-Atlantic Ridge, *Deep Sea Res., Part II*, *98*, doi:10.1016/j.dsr2.2013.10.005.

Armstrong, R. A., M. L. Peterson, C. Lee, and S. G. Wakeham (2009), Settling velocity spectra and the ballast ratio hypothesis, *Deep Sea Res., Part II*, *56*, 1470–1478, doi:10.1016/j.dsr2.2008.11.032.

Bailey, S., and P. Werdell (2006), A multi-sensor approach for the on-orbit validation of ocean color satellite data products, *Remote Sens. Environ.*, *102*(1–2), 12–23, doi:10.1016/j.rse.2006.01.015.

Behrenfeld, M., and P. Falkowski (1997), Photosynthetic rates derived from satellite-based chlorophyll concentration, *Limnol. Oceanogr.*, *42*(1), 1–20.

Berelson, W. M. (2002), Particle settling rates increase with depth in the ocean, *Deep Sea Res., Part I*, *49*, 237–251.

Brew, H. S., S. B. Moran, and M. W. Lomas (2009), Plankton community composition, organic carbon and thorium-234 particle size distributions, and particle export in the Sargasso Sea, *J. Mar. Res.*, *67*, 845–868.

Buesseler, K. O., and P. W. Boyd (2009), Shedding light on processes that control particle export and flux attenuation in the twilight zone of the open ocean, *Limnol. Oceanogr.*, *54*(4), 1210–1232.

Buesseler, K. O., et al. (2008), VERTIGO (VERtical Transport In the Global Ocean): A study of particle sources and flux attenuation in the North Pacific, *Deep Sea Res., Part II*, *55*(14–15), 1522–1539, doi:10.1016/j.dsr2.2008.04.024.

Chisholm, S. (1992), Phytoplankton size, in *Primary Productivity and Biogeochemical Cycles in the Sea*, edited by P. G. Falkowski, A. D. Woodhead, and K. Vivirito, pp. 213–237, Springer, USA.

Claustre, H., M. Babin, D. Merien, J. Ras, L. Prieur, S. Dallot, P. Ondrej, H. Dousova, and T. Moutin (2005), Towards a taxon-specific parameterization of bio-optical models of primary production: A case study in the North Atlantic, *J. Geophys. Res.*, *110*, C07S12, doi:10.1029/2004JC002634.

Cullen, J., P. Franks, D. Karl, and A. Longhurst (2002), Physical influences on marine ecosystem dynamics, in *The Sea*, edited by A. R. Robinson, J. J. McCarthy, and B. J. Rothschild, pp. 297–336, John Wiley, New York.

de Boyer Montégut, C., G. Madec, A. S. Fischer, A. Lazar, and D. Iudicone (2004), Mixed layer depth over the global ocean: An examination of profile data and a profile-based climatology, *J. Geophys. Res.*, *109*, C12003, doi:10.1029/2004JC002378.

de Boyer Montégut, C., J. Mignot, A. Lazar, and S. Cravatte (2007), Control of salinity on the mixed layer depth in the world ocean: 1. General description, *J. Geophys. Res.*, *112*, C06011, doi:10.1029/2006JC003953.

Deuser, W. G., F. E. Muller-Karger, and C. Hemleben (1988), Temporal variations of particle fluxes in the deep subtropical and tropical North Atlantic: Eulerian versus Lagrangian effects, *J. Geophys. Res.*, *93*(6), 6857–6682, doi:10.1029/JC093iC06p06857.

Deuser, W. G., F. E. Muller-Karger, R. H. Evans, O. B. Brown, W. E. Esaias, and G. C. Feldman (1990), Surface-ocean color and deep-ocean carbon flux: How close a connection?, *Deep Sea Res.*, *37*(8), 1331–1343.

Dunne, J., R. Armstrong, A. Gnanadesikan, and J. Sarmiento (2005), Empirical and mechanistic models for the particle export ratio, *Global Biogeochem. Cycles*, *19*, GB4026, doi:10.1029/2004GB002390.

Eppley, R. W., and B. J. Peterson (1979), Particulate organic matter flux and planktonic new production in the deep ocean, *Nature*, *282*, 677–680.

Fischer, G., et al. (2009), Mineral ballast and particle settling rates in the coastal upwelling system off NW Africa and the South Atlantic, *Int. J. Earth Sci.*, *98*, 281–298, doi:10.1007/s00531-007-0234-7.

François, R., S. Honjo, R. Krishfield, and S. Manganini (2002), Factors controlling the flux of organic carbon to the bathypelagic zone of the ocean. *Global Biogeochem. Cycles*, *16*(4), 1087, doi:10.1029/2001GB001722.

Guidi, L., L. Stemmann, G. A. Jackson, F. Ibanez, H. Claustre, L. Legendre, M. Picheral, and G. Gorsky (2009), Effects of phytoplankton community on production, size, and export of large aggregates: A world-ocean analysis, *Limnol. Oceanogr.*, *54*(6), 1951–1963.

Guidi, L., L. Legendre, G. Reygondeau, J. Uitz, L. Stemman, and S. Henson (2015), A new look at ocean carbon remineralization for estimating deepwater sequestration, *Global Biogeochem. Cycles*, *29*, 1044–1059, doi:10.1002/2014GB005063.

Helmke, P., S. Neuer, M. W. Lomas, M. Conte, and T. Freudenthal (2010), Cross-basin differences in particulate organic carbon export and flux attenuation in the subtropical North Atlantic gyre, *Deep Sea Res., Part I*, *57*(2), 213–227, doi:10.1016/j.dsr.2009.11.001.

Henson, S. A., R. Sanders, and E. Madsen (2012), Global patterns in efficiency of particulate organic carbon export and transfer to the deep ocean, *Global Biogeochem. Cycles*, *26*, GB1028, doi:10.1029/2011GB004099.

Honda, M. C. (2003), Biological pump in Northwestern North Pacific, *J. Oceanogr.*, *59*, 671–684.

Honda, M. C., H. Kawakami, K. Sasaoka, S. Watanabe, and T. Dickey (2006), Quick transport of primary produced organic carbon to the ocean interior, *Geophys. Res. Let.*, *33*, L16603, doi:10.1029/2006GL026466.

Honda, M. C., et al. (2015), Comparison of sinking particles in the upper 200 m between subarctic station K2 and subtropical station S1 based on drifting sediment trap experiments, *J. Oceanogr.*, *72*, 373–386, doi:10.1007/s10872-015-0280-x.

Honjo, S., J. Dymond, R. Collier, and S. J. Manganini (1995), Export production of particles to the interior of the equatorial Pacific Ocean during the 1992 EqPac experiment, *Deep Sea Res., Part II*, *42*(2–3), 831–870.
Honjo, S., S. J. Manganini, R. A. Krishfield, and R. Francois (2008), Particulate organic carbon fluxes to the ocean interior and factors controlling the biological pump: A synthesis of global sediment trap programs since 1983, *Prog. Oceanogr.*, *76*, 217–285, doi:10.1016/j.pocean.2007.11.003.
IOCCG (2014), Phytoplankton Functional Types from Space, Reports of the International Ocean-Colour Coordinating Group, No. 15, edited by S. Sathyendranath, IOCCG, Dartmouth, Canada.
Kawakami, H., and M. C. Honda (2007), Time-series observation of POC fluxes estimated from ^{234}Th in the northwestern North Pacific, *Deep Sea Res., Part I*, *54*, 1070–1090, doi:10.1016/j.dsr.2007.04.005.
Klaas, C., and D. E. Archer (2002), Association of sinking organic matter with various types of mineral ballast in the deep sea: Implications for the rain ratio, *Global Biogeochem. Cycles*, *116*(4), 1116, doi:10.1029/2001GB001765.
Krause, J. W., M. W. Lomas, and D. M. Nelson (2009), Biogenic silica at the Bermuda Atlantic Time-series Study site in the Sargasso Sea: Temporal changes and their inferred controls based on a 15-year record, *Global Biogeochem. Cycles*, *23*, GB3004, doi:10.1029/2008GB003236.
Lam, P. J., S. C. Doney, and J. K. B. Bishop (2011), The dynamic ocean biological pump: Insights from a global compilation of particulate organic carbon, CaCO 3, and opal concentration profiles from the mesopelagic, *Global Biogeochem. Cycles*, *25*, GB3009, doi:10.1029/2010GB003868.
Lampitt, R. S., and A. N. Antia (1997), Particle flux in the deep seas: Regional characteristics and temporal variability, *Deep Sea Res., Part I*, *44*(8), 1377–1403.
Lima, I. D., P. J. Lam, and S. C. Doney (2014), Dynamics of particulate organic carbon flux in a global ocean model, *Biogeosciences*, *11*(4), 1177–1198, doi:10.5194/bg-11-1177-2014.
Lomas, M. W., and S. B. Moran (2011), Evidence for aggregation and export of cyanobacteria and nano-eukaryotes from the Sargasso Sea euphotic zone, *Biogeosciences*, *8*(1), 203–216, doi:10.5194/bg-8-203-2011.
Lomas, M. W., N. Roberts, F. Lipschultz, J. W. Krause, D. M. Nelson, and N. R. Bates (2009), Biogeochemical responses to late-winter storms in the Sargasso Sea. IV. Rapid succession of major phytoplankton groups, *Deep Sea Res., Part I*, *56*(6), 892–908, doi:10.1016/j.dsr.2009.03.004.
Lomas, M. W., N. R. Bates, R. J. Johnson, A. H. Knap, D. K. Steinberg, and C. A. Carlson (2013), Two decades and counting—24-years of sustained open ocean biogeochemical measurements in the Sargasso Sea, *Deep Sea Res., Part II*, *93*(C), 16–32, doi:10.1016/j.dsr2.2013.01.008.
Longhurst, A. R. (2006), *Ecological Geography of the Sea*, 2nd ed., 560 pp., Academic Press, San Diego, Calif.
Lutz, M., R. Dunbar and K. Caldeira (2002), Regional variability in the vertical flux of particulate organic carbon in the ocean interior, *Global Biogeochem. Cycles*, *16*(3), 1037, doi:10.1029/2000GB001383.
Lutz, M. J., K. Calderia, R. B. Dunbar, and M. J. Behrenfeld (2007), Seasonal rhythms of net primary production and particulate organic carbon flux to depth describe the efficiency of biological pump in the global ocean, *J. Geophys. Res.*, *112*, C100110, doi:10.1029/2006JC003706.
Mackinson, B. L., S. B. Moran, M. W. Lomas, G. M. Steward, and R. P. Kelly (2015), Estimate of micro-, nano-, and picoplankton contributions to particle export in the northeast Pacific, *Biogeosciences*, *12*, 3249–3446, doi:10.5194/bg-12-3429-2015.
Malone, T. (1980), Algal Size, in *The Physiological Ecology of Phytoplankton*, edited by I. Morris, pp. 433–463, Blackwell Scientific Publications, Oxford.
Margalef, R. (1978), Life-forms of phytoplankton as survival alternatives in an unstable environment, *Oceanol. Acta*, *1*(4), 493–509.
Marsay, C. M., R. J. Sanders, S. A. Henson, K. Pabortsava, E. P. Achterberg, and R. S. Lampitt (2015), Attenuation of sinking particulate organic carbon flux through the mesopelagic ocean, *Proc. Natl. Acad. Sci. U.S.A.*, *112*, 1089–1094, doi:10.1073/pnas.1415311112.
Martin, J. H., G. Knauer, D. Karl, and W. Broenkow (1987), VERTEX: Carbon cycling in the northeast Pacific, *Deep Sea Res.*, *1*(34), 267–285.
McGillicuddy, D., A. Robinson, D. Siegel, H. Jannasch, R. Johnson, T. Dickey, J. McNeil, A. F. Michaels, and A. H. Knap (1998), Influence of mesoscale eddies on new production in the Sargasso Sea, *Nature*, *394*, 263–265.
Mignot, J., C. de Boyer Montégut, A. Lazar, and S. Cravatte (2007), Control of salinity on the mixed layer depth in the world ocean: 2. Tropical areas, *J. Geophys. Res.*, *112*, C10010, doi:10.1029/2006JC003954.
Montes, E., F. Muller-Karger, R. Thunell, D. Hollander, Y. Astor, R. Varela, I. Soto, and L. Lorenzoni (2012), Vertical fluxes of particulate biogenic material through the euphotic and twilight zones in the Cariaco Basin, Venezuela, *Deep Sea Res., Part I*, *67*, 73–84, doi:10.1016/j.dsr.2012.05.005.
Morel, A., and J.-F. Berthon (1989), Surface pigments, algal biomass, and potential production of the euphotic layer: Relationships reinvestigation in view of remote-sensing applications, *Limnol. Oceanogr.*, *8*, 1545–1562.
Mouw, C., and J. Yoder (2010), Optical determination of phytoplankton size composition from global SeaWiFS imagery, *J. Geophys. Res.*, *115*, C12018, doi:10.1029/2010JC006337.
Mouw, C. B., A. Barnett, G. McKinley, L. Gloege, and D. Pilcher (2016), Global Ocean Particulate Organic Carbon flux merged with satellite parameters, *Earth Syst. Sci. Data*, doi:10.5194/essd-2016-22.
Muller-Karger, F. E., M. Varela, R. Thunell, R. Luerssen, H. Hu, and J. Walsh (2004), The importance of continental margins in the global carbon cycle, *Geophys. Res. Let.*, *32*, L01602, doi:10.1029/2004GL021346.
O'Reilly, J. E. et al. (2000), *SeaWiFS Postlaunch Calibration and Validation Analyses, Part 3, NASA Tech. Memo. 2000-206892*, vol. 11, edited by S. B. Hooker and E. R. Firestone, 49 pp., NASA Goddard Space Flight Center.
Passow, U., and C. A. Carlson (2012), The biological pump in a high CO_2 world, *Mar. Ecol. Prog. Ser.*, *470*, 249–271, doi:10.3354/meps09985.
Pinckney, J. L., C. R. Benitez-Nelson, R. C. Thunell, F. Muller-Karger, L. Lorenzoni, L. Troccoli, and R. Varela (2015), Phytoplankton community structure and depth distribution changes in the Cariaco Basin between 1996 and 2010, *Deep Sea Res., Part I*, *101*, 27–37, doi:10.1016/j.dsr.2015.03.004.
Pomeroy, L. R. (1974), The ocean's food web: A changing paradigm, *BioScience*, *24*(9), 499–504.
Richardson, T. L., and G. A. Jackson (2007), Small phytoplankton and carbon export from the surface ocean, *Science*, *315*(5813), 838–840.
Romero, O. E., R. C. Thunell, Y. Astor, and R. Varela (2009), Seasonal and interannual dynamics in diatom production in the Cariaco Basin, Venezuela, *Deep Sea Res., Part I*, *56*(4), 571–581, doi:10.1016/j.dsr.2008.12.005.
Rousseaux, C. S., and W. W. Gregg (2015), Recent decadal trends in global phytoplankton composition, *Global Biogeochem. Cycles*, *29*, 1674–1688, doi:10.1002/2015GB005139.
Siegel, D. A., and W. G. Deuser (1997), Trajectories of sinking particles in the Sargasso Sea: Modeling of statistical funnels above deep-ocean sediment traps, *Deep Sea Res., Part I*, *44*(9–10), 1519–1541.
Siegel, D. A., K. O. Buesseler, and S. C. Doney (2014), Global assessment of ocean carbon export by combining satellite observations and food-web models, *Global Biogeochem. Cycles*, *28*, 181–196, doi:10.1002/2013GB004743.
Stemmann, L., and E. Boss (2012), Plankton and particle size and packaging: From determining optical properties to driving the biological pump, *Annu. Rev. Mar. Sci.*, *4*(1), 263–290, doi:10.1146/annurev-marine-120710-100853.
Thunell, R., C. Benitez-Nelson, R. Varela, Y. Astor, and F. Muller-Karger (2007), Particulate organic carbon fluxes along upwelling-dominated continental margins: Rates and mechanisms, *Global Biogeochem. Cycles*, *21*, GB1022, doi:10.1029/2006GB002793.

Timothy, D. A., C. S. Wong, J. E. Barwell-Clarke, J. S. Page, L. A. White, and R. W. Macdonald (2013), Climatology of sediment flux and composition in the subarctic Northeast Pacific Ocean with biogeochemical implications, *Prog. Oceanogr.*, *116*, 95–129, doi:10.1016/j.pocean.2013.06.017.

VLIZ (2009), Longhurst biogeographical provinces. [Available at http://www.marineregions.org/.]

Wetzels, R., and E.-J. Wagenmakers (2012), A default Bayesian hypothesis test for correlations and partial correlations, *Psychon. Bull. Rev.*, *19*, 1057–1064, doi:10.3758/s13423-012-0295-x.

Wilson, S. E., D. K. Steinberg, and K. O. Buesseler (2008), Changes in fecal pellet characteristics with depth as indicators of zooplankton repackaging of particles in the mesopelagic zone of the subtropical and subarctic North Pacific Ocean, *Deep Sea Res., Part II*, *55*, doi:10.1016/d.dsr2.2008.04.0149.

Wong, C. S., F. A. Whitney, D. W. Crawford, K. Iseki, J. R. Matear, W. K. Johnson, J. S. Page, and D. Timothy (1999), Seasonal and interannual variability in particle fluxes of carbon, nitrogen and silicon from time series of sediment traps at Ocean Station P, 1982–1993: Relationship to changes in subarctic primary productivity, *Deep Sea Res., Part II*, *46*, 2735–2760.

Xue, J., and R. A. Armstrong (2009), An improved "benchmark" method for estimating particle settling velocities from time-series sediment trap fluxes, *Deep Sea Res., Part II*, *56*(18), 1479–1486, doi:10.1016/j.dsr2.2008.11.033.

Yentsch, C., and D. Phinney (1989), A bridge between ocean optics and microbial ecology, *Limnol. Oceanogr.*, *8*, 1694–1705.